Multimedia Tools and Applications (2024) 83:77873–77944
https://doi.org/10.1007/s11042-024-18624-y

Feature subset selection through nature inspired computing for efficient glaucoma classification from fundus images

Law Kumar Singh[1] · **Munish Khanna**[2] · **Rekha Singh**[3]

Received: 26 September 2023 / Revised: 6 February 2024 / Accepted: 12 February 2024 /
Published online: 23 February 2024
© The Author(s), under exclusive licence to Springer Science+Business Media, LLC, part of Springer Nature 2024

Abstract

The selection of the most efficient features for glaucoma identification is the subject of our investigation because this disease is rapidly increasing worldwide. This disease causes lifelong blindness due to damage to the eye's optical nerve. Ophthalmologists have traditionally used tonometry, pachymetry, and other methods to measure intraocular pressure in order to diagnose patients. Yet each of these judgments takes time, requires high professional experience, and can be open to human error (inter-observer variability). Therefore, scholars are currently engaged in the domain of medical imaging, specifically focusing on the analysis of retinal images for the purpose of predicting glaucoma. This research also has the same objective and aims to address the aforementioned challenges. This empirical study proposes an artificial intelligence-based computer-assisted diagnosis (CAD) system which is built to overcome these difficulties by providing the best features for machine learning techniques for categorizing subject retinal pictures as "healthy" or "sick". This study presents a new set of reduced hybrid features that were selected from an initial set of 36 features extracted from fundus images of benchmark datasets that belonged to different classes to categorize patient fundus images into two categories: "healthy" or "infected." The nature inspired computing-based Emperor Penguin Optimization (EPO) algorithm and the Bacterial Foraging Optimization (BFO) algorithm are utilized to implement feature selection (FS) process. Additionally, a novel hybrid algorithm combining these two techniques is also proposed. Seven machine learning (ML) classifiers are engaged to compute eight statistically based performance metrics along with execution time computation, and a comparison of those metrics is also provided in a detailed fashion. The recommended method exhibits a fortunate performance with the highest specificity of 0.9940, sensitivity of 0.9347, and maximum accuracy of 96.55%. Expert medical practitioners who are overworked may receive assistance from the proposed system in making the optimal decisions to preserve human vision.

Keywords Feature extraction · Nature inspired computing based feature selection · Nature inspired optimization algorithms · Hybrid algorithm · Glaucoma detection · Medical data

Extended author information available on the last page of the article

1 Introduction

The extensive adoption of social media platforms and sensor technologies has led to the production of a significant amount of data with multiple dimensions. The dataset comprises a variety of features(characteristics) and the process of choosing the most appropriate features in relation to the target data is commonly known as feature selection (FS), which is also acknowledged as attribute(or characteristics) subset selection [1]. The procedure of FS is of utmost importance in the identification and extraction of the most pertinent information from a given dataset. When dealing with high-dimensional data, it becomes less useful to use regression, classification, and clustering methods. This is mostly because the spatial and temporal complexity increases significantly. The dataset encompasses various features, some of which may exhibit redundancy or insignificance. Duplicate and irrelevant features are detrimental to a classifier's effectiveness. Therefore, it is common practice to employ FS techniques in order to identify the most suitable subset of features from datasets that have a high number of dimensions as a means of addressing this problem. The procedure of FS plays a vital role in accurately identifying and extracting the most pertinent and valuable information from a provided dataset. Feature selection is a method employed to enhance the accuracy of learning and improve the clarity of results by eliminating redundant and noisy data from datasets with high dimensions [2]. By utilizing FS techniques, the ML algorithm can be trained with improved efficiency and simplicity. In addition, it efficiently addresses the issue of over-fitting and decreases the complexity of the classifier, thereby improving its comprehensibility [3]. Hence, it is crucial to utilize a suitable mining methodology to extract the fundamental characteristics (features) from the dataset. Previous studies have utilized various meta-heuristic techniques to effectively reduce the dimensionality of the feature space. The utilization of technology facilitates the acceleration of computational processes and improves the accuracy of categorization. The effectiveness of classifiers might be hindered by feature spaces that include a substantial number of duplicate or insignificant features. To enhance the efficiency of the classifiers, FS methods are used to eliminate redundant characteristics from the initial collection. These techniques facilitate the process of identifying the most suitable subset of features. FS is a commonly utilized methodology in the domain of CAD that seeks to determine the relevant attributes that have a significant impact on the accuracy of classification. In order to ensure optimal performance of the classification subsystem, features that have minimal influence are excluded to mitigate any potential negative effects. The primary objective of the FS subsystem is to address the issue of duplicate features by strategically identifying and preserving the most advantageous subsets of features in the dataset. Hence, the integration of FS will greatly enhance the accuracy and efficiency of the CAD system.

As a result of the investigation of this experimental study, glaucoma, which is also known as the "silent thief of vision," was first identified as a medical condition in the early 17th century. This was the time when the word "glaukeoma" was first used in ancient Greece. The term "cataract" is derived from the Greek words "obscurity of the lens" and "cataract," and it denotes a lack of knowledge or awareness of this condition. On a global scale, glaucoma is regarded as the second most frequent major cause of blindness. This condition is the second most common cause of irreversible vision loss, right after cataracts. There is a chance that it will supplant cataracts as the main etiological factor in the absence of medical treatment. Glaucoma is thought to affect around 60 million people worldwide and is expected to significantly increase to around 79.6 million by the year 2023 [4]. The World Health Organization estimates that glaucoma affects more than 60 million people

worldwide and could affect as many as 80 million people in the near future. Additionally, it has been estimated that this issue affects 12 million people in India, which is a sizable population. Common symptoms of this condition include an abrupt onset of visual impairment, severe ocular discomfort, decreased visual clarity, irritated ocular organs, and the observation of halos surrounding light sources [5]. People over the age of 40 are more likely to experience the symptoms of this illness. The ability of the human brain to interpret and comprehend the surrounding environment comes from its ability to receive visual information from the retina and transmit it to the brain via the optic nerve. Increased intraocular pressure causes the optic nerve to be damaged, which causes the illness to begin. Visual impairment, ocular discomfort, decreased visual acuity, ocular irritation, and the observation of haloes around light sources are typical acute manifestations [6, 7]. Glaucoma has the potential to cause the optic nerve to suffer irreparable damage in the absence of proper medical intervention, which would subsequently worsen visual acuity. Therefore, it is essential to emphasize the significance of early glaucoma detection because this significantly reduces the risk of permanent vision loss.

A fundus camera captures eye images (Fig. 1). Fundus cameras use a microscope and light to image the retinal fundus. The fovea, macula, optic disc, and optic cup are fundus region structures. Since it's noninvasive, it's an effective eye health test. The optic disc appears yellowish in colored fundus imaging, separated between the inner optic cup and the outside neuroretinal rim (outer boundary). Detection of glaucoma is performed via the optic nerve cup or by extending it. The most accurate glaucoma indication is the

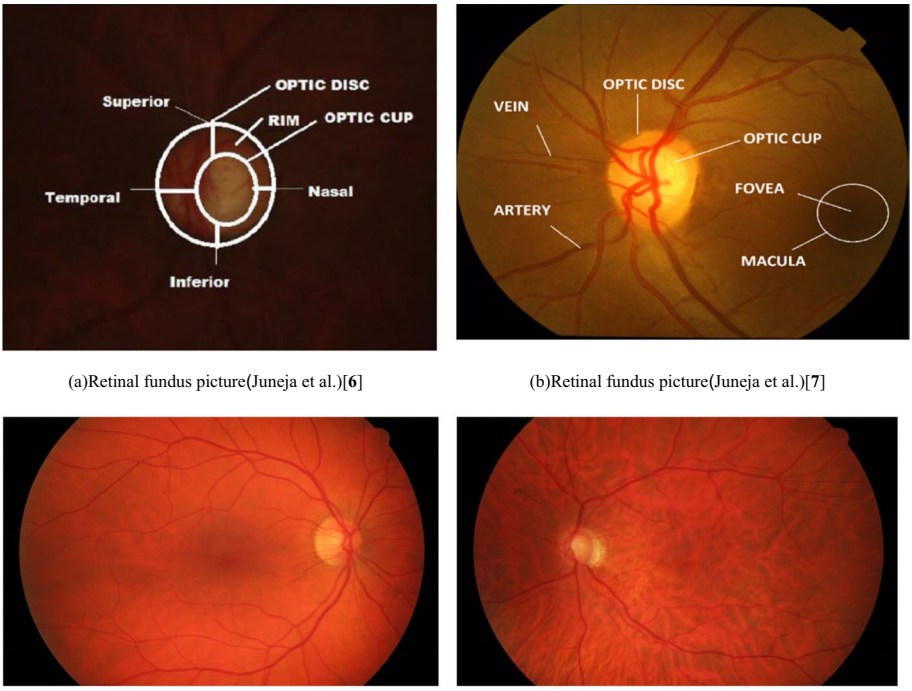

(a)Retinal fundus picture(Juneja et al.)[**6**] (b)Retinal fundus picture(Juneja et al.)[**7**]

(c) Retinal picture of non-infected individual (d) Retinal picture of infected(glaucomatous) individual

Fig 1 Retinal fundus pictures

cup-to-disc ratio (CDR), which is the ratio of the optic cup diameter to the optic disc diameter. Doctors diagnose glaucoma if the CDR is 0.65 or higher [8]. These medical practitioners must physically extract discs and cups from individual photos, making their methods slow, arduous, and unsuccessful. Professional graders can measure, record, and diagnose glaucoma in eight minutes per eye. To detect glaucoma in the retina, ophthalmologists use pachymetry, tonometry, perimetry, gonioscopy, and ophthalmoscopy. While ophthalmoscopy examines the optic nerve's color and structure, tonometry analyzes the pressure within the eye. By using gonioscopy, perimetry, and pachymetry, it is possible to measure the iris-cornea angle, the visual field, and the cornea's thickness. All of these methods require a lot of time and human labor and have the potential to produce assessments that are subject to the biases displayed by various experts (vulnerable to human errors) [9]. An automated glaucoma diagnosis method is necessary to overcome existing techniques' limitations. Computers foresee medical concerns using non-invasive imaging. CAD systems are used to solve the classification problem. For diagnostic glaucoma screening, a CAD system may minimize computational complexity. Ophthalmologists need a second-opinion CAD system to save time. It may minimize misclassification, relieve doctors, and improvise inter- and intra-observability. CAD systems can identify several retinal fundus traits, forecast glaucoma, and categorize retinal images as "normal" or "abnormal."

The number of patients with this disease is increasing at a very fast pace; as per the characteristics of this disease, the infection leads to irreversible blindness [10]. The infection must thus be identified as soon as possible in order to begin therapy promptly and stop the rate of visual loss (or at least reduce it). Traditional ophthalmological exams and procedures take time and are subject to intra-observer variability. Moreover, manually computing the optic disc, cup, and cup-to-disc ratio by ophthalmologists is a common, labor-intensive, and error-prone operation. It is widely acknowledged that glaucoma is a progressive condition that leads to the deterioration of the optic nerve, which plays a crucial role in transmitting visual stimuli from the eye to the brain. Patients typically do not notice any vision problems in the early stages of glaucoma, so they are unaware that they have the disease. By impairing peripheral vision in its severe stages, glaucoma can result in permanent blindness. But glaucoma may be slowed down and properly treated to help prevent visual loss if it is discovered early. To aid in the early discovery of the condition, those who are suspected to be suffering from glaucoma should have routine eye exams. In order to identify whether or not glaucoma symptoms are present, an ophthalmologist will physically examine a patient's retina during an eye exam. It could take a long time to manually analyze retinal pictures. In order to ensure the accuracy of the diagnosis, ophthalmologists with sufficient experience should also review the images. In light of the fact that expert ophthalmologists would have to analyze a significant number of patient photos, the majority of which lack any signs of illness, frequent manual screening would be exceedingly burdensome on them. By collecting, analyzing, and categorizing retinal images independently, automated screening technology provides a way to get around these limitations. As a result, it can only make suggestions for people who show signs of glaucoma and are in need of medical attention. Because of all of these considerations, we are motivated and inspired to provide a reliable glaucoma CAD system that takes very little human interaction and time to confirm this infection. This system inputs the potential patient's fundus photos and classifies each image as either "healthy" or "infected."

It is essential for every human disease classification system to first determine which of its most valuable components should be preserved before removing any extraneous or redundant parts. The feature collection's capacity to forecast outcomes may be compromised if there are a significant number of irrelevant or undesirable features [11]. The

decision about the best features is very vital. As a result, the classifier's capacity for making precise predictions is increased while the associated computational costs are decreased [12]. This assertion encourages and inspires us to continue working on the creation of an ideal feature set, specifically in the context of dimension reduction, with the goal of identifying glaucoma. The technique being discussed aims to improve the performance of the classification system by reducing the feature space [13]. A glaucoma prediction system's design process for feature selection is of utmost importance. Either a soft computing-based approach or a methodology with a statistical foundation is typically used in the field of FS. In order to address the current issue, the present study uses three nature inspired computing methodologies, specifically the EPO algorithm, the BFO algorithm, and their hybrid. The BFO algorithm has been selected due to several advantages like balancing exploration and exploitation, its adaptability, sturdiness, robustness, adaptive strategy, simplicity, ease and effectiveness, efficiency, frequently converges towards optimal solutions, scalability and parallelism and relevance which motivates us to select this algorithm. Similarly, the EPO algorithm also has been shortlisted due to its advantages like efficiency, balancing between global and local search, adaptive mechanisms, flexibility and mechanism, optimal convergence, social interaction modeling, solving capability of engineering problems. Hybridization of nature inspired algorithms is a viable strategy in a variety of computational applications because it provides several benefits such as enhanced performance, higher robustness, better solution quality, and flexibility to multiple issue scenarios. However, the limitations of BFO include sensitivity to parameter changes, computational overhead, chance of local optima trapping, strict investigation in complicated environments, no convergence guarantee, performance variability and problems with scalability. Similarly, EPO algorithm exhibit limitations like insufficient validation, restricted empirical research, sensitivity to parameters (configurations), convergence speed and solution quality, restricted application scope, challenges in execution and optimization performance: efficiency and scalability. As far as is known, these three algorithms haven't been used very often to diagnose diseases that affect humans, like glaucoma. Benchmark fundus images that are widely used in the field are used to evaluate the proposed technique. The goal of the suggested methodology is to increase classification accuracy by using a feature selection strategy that reduces the number of features used and the error rate. Its use is intended to identify the most beneficial set of characteristics for the specified task. Using particular and hybrid data transformation techniques, the benchmark dataset's attributes are chosen to produce the greatest benefit. Six classifiers that are based on machine learning have been selected for analysis in order to compare the chosen attributes of these three methodologies. Fundus images taken from a benchmark dataset are used to evaluate the proposed methodology. There has been a total of twelve experiments. More than half of the attributes are excluded in a sizable portion of cases. A cut-short of up to 88.88% of initial extracted features is possible under ideal circumstances. When four of the original 36 characteristics are reclaimed without having a significant effect on accuracy, this decline can happen. In order to achieve a balanced and ideal combination of global and local search strategies, as well as exploration and exploitation techniques, a hybrid algorithm is used. To make feature selection and classification in fundus images efficient, the suggested methodology combines the BFO and EPO algorithms.

The aim of the study is to propose a novel, computer-based novel efficient, and fast feature selection approach that can select an optimal subset of features from the initial extracted features that are required for the prediction of human disease. Although many studies have been published in last decade on efficient feature selection approach but there is still a scope of improvements in classification results and computation time.

One of the most important aspects of the data mining and machine learning fields is feature selection, which involves eliminating unnecessary data in order to choose the optimal subset of features for the target data. Nevertheless, choosing the best set of features from a dataset using conventional feature selection techniques is difficult because there are 2^n feature subsets that can be chosen for every n features. Thus, this study presents a new feature selection strategy based on soft-computing approaches for effective classification of healthy vs infected humans.

Even with the number of research on effective feature selection techniques published in the past ten years, there is still room for improvement in terms of computation times and classification accuracy. Other challenges include reduction of higher dimensionality data, selection of relevant features and removing of redundant features, computational complexity of the approach, overfitting and generalization, interability and explainability of the selected features, and dynamic nature of the disease under investigation.

An extremely effective soft-computing dependent method for predicting human disease was suggested by this empirical study. These algorithms have proven useful in solving various engineering problems, but they are rarely applied to the classification of human diseases, particularly the prediction of glaucoma. Additionally, we have proposed a new algorithm that combines two well-known prior algorithms. Its performance is compared to these two prior algorithms. Additionally, a new dataset consisting of a combination of images from various benchmark image datasets is created. Additionally, this dataset is larger than many of the benchmark datasets that are currently in use Tables 1, 2, 3, 4, 5, 6, 7, 8, 9, 10, 11, 12, 13, 14, 15, 16, 17 and 18.

The empirical study presented in this research aims to tackle the aforementioned issues by first identifying the optimal and most effective features required for the diagnosis of glaucoma, a prevalent eye disease. The study concludes by demonstrating exceptional performance and outcomes. The main contribution of this study can be summarized as follows:

- Based on a comprehensive review of the existing literature, it is evident that there exists significant potential for feature optimization in the context of glaucoma identification. A proposed feature selection strategy, referred to as the BFOEPO hybrid, is introduced by considering the advantages of both BFO and EPO. This approach has the potential to eliminate redundant and superfluous features within the feature space, thereby enhancing the accuracy of classification and reducing computational costs. Based on our current understanding, we are at the forefront of utilizing these algorithms for the purpose of identifying glaucoma, thereby addressing a significant void in existing research.
- The primary purpose of the FS strategy is to enhance the accuracy of categorization while simultaneously minimizing the count of shortlisted features and reducing the error rate. To achieve this, the strategy employs specified and hybrid data transformation techniques to obtain the optimal subset of attributes (features) from a combination of various standard datasets.
- Twelve tests have been conducted as part of a series of thorough experiments. Our customized dataset also stands out as one of the largest when compared to the most recent state-of-the-art research shown in Table 19. Furthermore, this study presents a thorough examination of various parameters in order to showcase the practicality of the proposed method. In addition to the evaluation of confusion metrics and ROC curves, the efficiency of six machine learning classifiers has been assessed through the computation of eight efficiency measurement parameters. These parameters serve as indica-

Table 1 Comparative table previous of 25 state-of-the-art studies

Reference and Year	About dataset and Images	About Features	Approach Used	ML-classifier/DL-Model	Results
Acharya et al. [48]	Private 60 fundus images	Non-structural HOS and Textural features	Feature extraction, FS and supervised classification	Random Forest	Accuracy-90.00%
Dua et al. [49]	Private 60 fundus images	Non-structural wavelet features	Feature extraction, Feature selection (Chi-squared, Gain Ratio and Information Gain Feature Evaluation and Relief Feature Ranking) and supervised classification	Support vector machine (SVM)	Accuracy-93%(around)
Mookiah et al. [50]	Private 60 fundus images	Non-structural HOS and wavelet features	13 statistically significant features (using HOS and wavelet) extracted followed by supervised classification	SVM	Accuracy-95.00%; Sensitivity 0.9333 Specificity 0.9667;
Noronha et al. [51]	Private 272 fundus images	Non-structural HOS features	3^{rd} order HOS cumulants followed by FS using principal component analysis (PCA), linear discriminant analysis (LDA) and independent component analysis (ICA) techniques and then classification through ML.	Naïve Bayes	Accuracy-92.65%; Sensitivity 1.000 Specificity 0.9200;

Table 1 (continued)

Reference and Year	About dataset and Images	About Features	Approach Used	ML-classifier/DL-Model	Results
Acharya et al. [52]	Private 510 fundus images	Non-structural gabor features	Feature extraction followed by feature ranking(t-test, Bhattacharyya space algorithm, Wilcoxon test, Receiver Operating Curve (ROC) and entropy ranking methods) techniques and then classification through ML	SVM	Accuracy-93.10%; Sensitivity 0.8975 Specificity 0.9620;
Issac et al. [53]		Structural features like disc damage likelihood scale (DDLS) and cup to disc ratio (CDR)	Classification using SVM and neural network (NN).	SVM	Accuracy-94.11%; Sensitivity 1.000
Salam et al. [54]	2 Private datasets of 50 and 100 fundus images respectively	Structural (optic cup and optic disc followed by CDR calculation), 5 texture and 2 intensity features	Feature extraction followed by principal component analysis for feature selection and then classification	SVM	Sensitivity 1.000 Specificity 0.870;
Haleem et al. [55]	RIM-ONE (124 images)	Structural, Dyadic Gaussian, gabor and wavelets features	The proposed methodology involves first performing feature extraction, followed by wrapper feature selection, and afterwards using different kinds SVMs for classification purposes.	Twin SVM	Accuracy-94.4%; Sensitivity 0.923 Specificity 0.953;

Table 1 (continued)

Reference and Year	About dataset and Images	About Features	Approach Used	ML-classifier/DL-Model	Results
Claro et al. [56]	RIM-ONE , DRISTHI-GS and DRIONS-DB . with 169, 50 and 110 pictures respectively.	Structural and textural features; Haralick set 14 significant features, Contrast, Homogeneity, Correlation, Entropy and Energy	Feature extraction and classification	Multi Layer Perceptron	Accuracy-93.03% Recall-0.9300 Precision-0.9300 F-Score-0.9290 Kappa-0.8000
Singh et al. [20]	63 private images	Wavelet features extraction followed by grading of these features	Wavelet feature extraction has been followed by prominent FS using evolutionary attribute selection/ PCA. Finally, Glaucoma image classification	SVM	Accuracy-95.24%; Sensitivity 0.9687 Specificity 0.9333;
de Sousa et al. [57]	455 images of version 2 of RIM-ONE dataset	Geostatistical features were extracted and considered	Local Binary Pattern (LBP) to represent the optic disk region and Geostatistical features extraction followed by classification using GA and SVM	SVM	Accuracy-91.00%; Sensitivity 0.9500 Specificity 0.8820;
Koh et al. [58]	1486 private images	Wavelet features extraction (Nonlinear features like entropies and energy retrieved from the scalogram images of 2D-CWT. Fuzzy , Shannon , Kapoor , Renyi and Yager entropies were extracted.	Feature extraction followed by feature selection (15 features selection) using particle swarm optimization and the finally classification using Random Forest. 10 fold cross validation was implemented	Random Forest	Accuracy-92.48%; Sensitivity 0.8937 Specificity 0.9558;

Table 1 (continued)

Reference and Year	About dataset and Images	About Features	Approach Used	ML-classifier/DL-Model	Results
Septiarini et al. [59]	84 private images	Statistical features considered	Mean, smoothness and 3rd moment are extracted from images of the optic nerve head; After that FS using the correlation method.	K-Nearest Neighbour	Accuracy-95.24%; Sensitivity- 0. 9512 Specificity-0.9535; AUC-0.93
Selvathi et al [60]	45 private images	Wavelet features extracted and considered	The wavelet channels utilized are daubechies, symlet3. These channels are inspected by utilizing a standard 2-D Discrete Wavelet Transform (DWT). Average or mean, Energy, Standard deviation, Variance are computed followed by image classification	Neural Network	Accuracy-95.63%;
Kanse et al. [61]	45 images from HRF dataset	Features from pre-processed image (mean, variance, entropy, skewness and kurtosis) optical disk features (mean, variance, entropy, bright pixel count and INST) and features from segmented vessel images (mean, variance, entropy)	Four major steps, (1) pre-processing, (2) proposed hybrid feature extraction, (3) segmentation and (4) Classification through the proposed harmonic genetic-based support vector neural network (HG-SVNN) classifier.	HG-SVNN classifier	Accuracy-90.00%; Sensitivity-0.9333; Specificity0.8666 ;

Table 1 (continued)

Reference and Year	About dataset and Images	About Features	Approach Used	ML-classifier/DL-Model	Results
Kirar et al. [43]	505 MIAG fundus images dataset	Pictures are divided into approximation and detail coefficients by DWT, and subband pictures by EWT.	Concatenated features are obtained from the DWT, EWT, DWTEWT, and EWTDWT. Out of 308, 60 ranking characteristics were chosen and put into the singular value decomposition (SVD).	14 features are fed to SVM	Accuracy-83.57%; Sensitivity-.8640; Specificity0.8080 ;
Agrawal et al. [24]	505 fundus images of MIAG images database	The QB-VMD SBIs (quasi-bivariate variational mode decomposition-sub-band images) are used to extract features. Zernike moment, Hu's Invariant Moments, chip histogram, texture features utilizing grey-level co-occurence matrix, haralick texture features, GLCM Features, and grey-level run length matrix were among the 75 attributes that were retrieved.	Using the reliefF approach, 45 features were selected and sent to SVD for dimensionality reduction.	17 features forwarded to Least squares SVM (LS-SVM).	Accuracy-86.13%; Sensitivity-.8480; Specificity0.8743 ;
Renukalatha et al. [62]	100 retinal images of RIM ONE database	Structural and non-structural features (including texture, kurtosis ,skewness, contrast, energy, correlation, entropy ,variance, standard deviation, and mean)	Region of interest and feature extraction was performed. For classification Naïve Bayes binary classifier and simplified multiclass SVM (Sim-MSVM) were implemented.	SVM	AUC upto 0.8919

Table 1 (continued)

Reference and Year	About dataset and Images	About Features	Approach Used	ML-classifier/DL-Model	Results
Jerith & Kumar [63]	Not Reported	GLCM(Grey Level co-occurrence matrix), Speeded up Robust feature(SURF), Histogram of oriented gradients(HOG) features and global features	Feature selection through gray wolf algorithm	Neural Network	Accuracy-93.103%; Sensitivity 0.9167 Specificity 0.9411
Krishnamoorthi, & Chinnababu [64]	570 images of DRISHTI-GS , FAUand RIM-One	Non-morphological spatial characteristics such as local binary patterns, directed gradient histograms, and fractal features	Feature selection through Sequential floating forward selection method	SVM	Best accuracy of 91.05% for RIM-One
Araújo et al. [65]	455 images of second version of RIM-ONE database	Diversity indexes as texture descriptors	Shannon (29 features) and McIntosh (31 features) diversity indexes for feature extraction, GA for feature selection.	SVM	Accuracy-93.410%; Sensitivity 0.9283 Specificity 0.9369
Thakur and Juneja[66]	DRISHTI-GS and RIM-One	61 features (DDLS, CDR, GLRM, GLCM, HOS, FoS, HOC and Wavelets) extracted	10 features selected using Information Gain, Gain ratio, Co-relation, Relief feature ranking and wrapper selection	SVM	Accuracy-97.22%; Precision 0.97; Sensitivity 0.97 Specificity 0.96;
Elangovan et al. [67]	RIM-ONE and DRIONS-DB	Cup-to-disk ratio(CDR) and statistical features such as cup entropy, rim entropy, and kurtosis.	Optic discs and cups are segmented using an improved FCM algorithm based on morphological reconstruction and membership filtering (FRFCM). The segmented findings are used to determine the CDR.	It is discovered that the average CDR error is 0.0402, the cup entropy error is 0.0473, the rim entropy error is 0.0462, and the kurtosis error is 0.0570.	Classifications based on cup entropy and kurtosis showed 98.57% success rates. CDR classification and rim entropy classification both had success rates of 92.85% and 87.14%, respectively.

Table 1 (continued)

Reference and Year	About dataset and Images	About Features	Approach Used	ML-classifier/DL-Model	Results
Kirar et al. [68]	505 images of RIM-ONE	Image channels (ICs) and second level DWT from fundus images	Feature extraction followed by dimension reduction using singular value decomposition (SVD), later on classification is performed by ML classifier. 10 fold cross validation was implemented	Least squares SVM	Accuracy-84.95%; Sensitivity-.8600; Specificity0.8385 ;
Khan et al. [69]	455 images of RIM-One of MIAG (Medical Image Analysis Group,n.d.).	8 features extracted (Contrast,Mean, Homogenity,Energy, Entropy, Variance, RMS, Standard Deviation)	Feature selection using T-Test, Bhattacharyya Distance method, Entropy Ranking method, Neighbourhood Component Analysis,Receiver Operating Characteristics (ROC) method, Wilcoxon rank-sum test method	Least squares SVM	Accuracy-91.22%; MCC-0.7263; Sensitivity-.8551; Specificity0.9850 ;

Table 2 List of images utilized for performance evaluation

S No.	Name of the dataset	Images Selected
1.	ACRIMA	396 infected cases and 309 normal cases
2.	DRISHTI	16 infected cases
3.	HRF	15 infected cases and 15 normal cases
4.	ORIGA	168 infected cases and 482 normal cases
5.	Private	631 infected cases and 1080 normal cases

tors of the classifiers' performance in terms of efficiency. The implementation effort of this split approach also demonstrates the temporal requirements associated with the execution of a nature inspired-computing technique and the training and testing of a machine learning model.

- In addition, we have also disclosed the extended results as three tables that show the ideal values attained for eight efficiency assessment criteria. Based on the selection of the lowest number of features for each of the three techniques, these values were produced by six machine learning classifiers. In previous state-of-the-art studies, this specific table is seldom ever seen.
- This study aims to offer researchers the most informative features, including an effective and expedient support system for ophthalmologists that can be relied upon. Additionally, it seeks to provide a software-based tool that can aid in mitigating the decline of human eyesight by enabling early, efficient, and effective identification of ocular infections. The tool has the capability to be modified for compatibility with mobile and wearable medical equipment, thereby enabling its utilization in settings characterized by a scarcity of proficient medical professionals.

The organization of this research study is enumerated as follows: The second section is devoted to a consideration of prior relevant works. The datasets and methods are described in Section 3, whilst the findings and analyses are described in Section 4. In Section 5, comparisons with current state-of-the-art investigations are presented. In Section 6, the conclusion of the study is demonstrated.

2 Prior studies

The authors of study [14] use the stacking ensemble learning technique to create a deep ensemble model. There were thirteen pre-trained models used. Multiple different settings, comprising five classification methods and thirteen convolutional neural network (CNN) designs, had their performance evaluated. An ensemble selection approach with two stages was developed to find the best combinations. A technique of probability averaging was used to merge a few combinations. The final classification was determined using an SVM classifier. This empirical study [15] demonstrated a method for accurate retinal vessel detection from fundus images using a generative adversarial network (GAN) with several loss functions. The proposed GAN architecture consists of a classification network for the discriminator and a segmentation network for the generator. The discriminator is a vision transformer acting as a binary classifier, while the generator is a multi-scale residual CNN

Table 3 List of features retrieved from fundus images

S. No.	Features	S. No.	Features	S. No.	Features
1	CDR (Cup Disc Ratio)	13	mat0_avg	25	DWT (Discrete Wavelet Transform)
2	GLCM0 (Grey Level Co-occurrence Matrix)	14	mat45_avg	26	FOS (First Order Statistical)
3	GLCM45	15	mat90_avg	27	Cum2est
4	GLCM90	16	mat135_avg	28	Coherence
5	GLCM135	17	GLRM 0(Grey Level Run Length Matrix)	29	Bicoherence
6	SRE (Short Run Emphasis)	18	GLRM 45	30	Spectrum
7	LRE (Long Run Emphasis)	19	GLRM 90	31	Energy
8	GLU (Grey Level Uniformity)	20	GLRM 135	32	Homogenity
9	RLU (Run Level Uniformity)	21	HOS (Higher Order Spectral)	33	Corelation
10	RPC (Rational Polynomial Coefficient)	22	NRR (Neuro Retinal Rim)	34	Contrast
11	mat0	23	DDLS (Disc Damage Likelihood Scale)	35	Dissimilarity
12	mat45	24	HOC (Higher Order Cumulant)	36	Entropy

Table 4 Experiments settings

Size of the Population	5, 10, 15, 20
No. of features	36
No. of samples	3112
Upper Bound	1
Lower Bound	0
Times of elimination	2
Times of reproduction	4
Maximum length of swim	5
Rate of Elimination	0.25
Mutation rate	0.08
Selection method	Essential selection
Crossover type	One-site crossover

with skip connections and upsampling. The inception module collects fine vessel segment scales as well as multiscale vessel segment parameters. Stacking self-attention networks and positionally completely connected feed-forward networks are used to infer two-class output. The attention mechanism of the transformer was capable of discriminating and preserving both global and local information. The suggested GAN model splits the blood arteries more accurately using adversarial learning to provide cutting-edge results. A contrast-limited adaptive histogram equalization approach enhances the contrast of blood vessels during preprocessing. In [16],the segmentation models include three different CNN backbones: Inception-v3, visual geometry group 19 (VGG19), and residual neural network 50 (ResNet50). They are based on an attention U-Net. The three CNN architectures mentioned above are changed and used in the classification models as well. In [17] the idea behind this is to provide a novel pre-processing method that uses Gaussian filtering to help remove undesirable noise from photos. The Modified Level Set Algorithm is then used to segment the Optic Cup. Segmentation is followed by the derivation of morphological (disc area, cup area, and blood vessel) and non-morphological (color, shape, and modified LBP) properties. 5 to 100 micrometers is the range of blood vessel thickness. The weights are then adjusted using the Self Adaptive Butterfly Optimization Algorithm, and these features are subsequently categorized using the adjusted CNN framework. In this study[18], a quick segmentation technique for the segmentation of the optic disc and the arteries of the retina is suggested. It is based on a novel simplified U-Net design. The redesigned and strengthened structure of the suggested technique would shorten prediction times while keeping performance and accuracy on par with existing cutting-edge approaches. In [19], a deep neurofuzzy network (DNFN)-based technique for glaucoma detection is introduced. The retinal picture is first input for noise-removal preprocessing. Then, the DeepJoint model and the blackhole entropy fuzzy clustering technique are used, respectively, to segment blood vessels and identify the optic disc (OD). OD and blood vessels are then supplied to the DNFN, which is then trained using the newly developed MultiVerse Rider Wave Optimization (MVRWO). The recently created MVRWO combines the MultiVerse Optimizer, Rider Optimization Algorithm, and Water Wave Optimization. The output is then categorized using the DNFN's loss function.

Wavelet feature extraction occurred first in study [20], followed by genetic feature optimization, a few learning strategies, and several parameter settings. The segmented, blood vessel-free optic disc used in this work is used to extract characteristics. The wavelet

Table 5 List of parameters used in BFO algorithm

Parameter	Description	Parameter	Description
Q	Bacterial number	$\aleph_d^j$	The d th component of the $\aleph^j$
$\aleph$	A bacterium on the optimization domain	$\aleph^j(k,l,m)$	The j th bacterium in the k th chemotaxis l th elimination-dispersal procedure
$\aleph^j$	The j th bacterium position	$\Delta(j)$	A random value on [-1, 1] for the j th bacterium
r_{attract} and x_{attract}	Coefficients of attraction-repulsion	$h1_{\text{repellant}}$ and $x_{\text{repellant}}$	Coefficients of repulsion-repulsion
$Bcc\left(\aleph, \aleph^j(k,l,m)\right)$	Cell to cell communication value	Q_r	Number of population members ,have sufficient nutrients

Table 6 Information about features selected with population size (PS) 5, 10, 15 and 20 through 70:30 split approach

Number of features (NoF)	Number of iterations (NoI)	Population size (PS)	Features Selected (FSel)	Features number (FNo.)	Fitness value (FV)	Execution Time (ET)
Experiment 1: Performance on Population size 5						
36	300	5	4	11, 18, 23, 28	**0.8239**	1.8368
Experiment 2: For population size 10						
36	200	10	9	1, 4, 6, 11, 13, 28, 30, 33, 34	**0.8760**	2.2595
Experiment 3: For population size 15						
36	500	15	12	2, 4, 6, 11, 14, 16, 20, 24, 29, 31, 35, 36	**0.7880**	5.0142
Experiment 4: For population size 20						
36	300	20	15	2, 5, 10, 13, 17, 20, 21, 22, 24, 26, 29, 30, 33, 34, 35	**0.8092**	7.4664

Table 7 Performance of implemented six ML classifiers on varying PS from 5 to 20 (70:30 Splitting Approach)

Classifier	Specificity	Sensitivity	Precision	F1-score	Kappa score	MCC	AUC value	Accuracy	Execution Time	Standard Deviation	*p*-value (two tailed test)
Experiment1: Comparing the outcomes of different ML models on selected attributes with minimal cost **0.82390** (PS 5)											
Logistic Regression (LR)	0.994	0.663	0.9838	0.7922	0.7089	0.7369	0.9417	87.644	0.4755	87.844 ± 0.69	0.31543
Random Forest(RF)	0.973	0.826	0.944	0.8811	0.8222	0.8263	0.9516	**92.084**	1.3667	92.084 ± 0.28	0.313543
Decision Tree(DT)	0.9431	0.7282	0.8758	0.7952	0.6977	0.7042	0.8764	86.679	0.2442	86.679± 1.06	0.282285
Support Vector Machine (SVM)	0.982	0.7771	0.9597	0.8588	0.793	0.8026	0.9423	90.926	0.3239	90.926± 0.54	0.312831
K-Nearest neighbor (KNN)	0.958	0.8043	0.9135	0.8554	0.7834	0.787	0.9326	90.347	3.0573	90.347± 0.32	0.308203
XGBoost	0.99	0.809	0.9723	0.839	0.8002	0.7901	0.932	89.987	0.9988	89.987± 0.06	0.307918
Ensemble	0.9888	0.7132	0.9701	0.8322	0.7402	0.7603	0.9291	88.803	1.2119	89.987± 0.26	0.306544
Experiment 2: Comparing the outcomes of different ML models on selected attributes with minimal cost **0.87603** (PS 10)											
LR	0.9647	0.8483	0.92638	0.8856	0.8296	0.8314	0.8946	92.471	0.5344	92.471±0.33	0.29001
KNN	0.9647	0.8707	0.92814	0.8985	0.8479	0.8489	0.9324	**93.243**	1.411	93.243±0.62	0.307586
DT	0.9029	0.8089	0.81355	0.8112	0.7128	0.7128	0.9129	87.065	0.2634	87±1.70	0.298433
SVM	0.947	0.882	0.89714	0.8895	0.8324	0.8324	0.942	92.471	0.3437	92.471±0.33	0.31216
RF	0.9642	0.8651	0.92771	0.8953	0.8434	0.8445	**0.9527**	93.05	1.4137	93.050±0.55	0.308868
XGBoost	0.9342	0.8331	0.9007	0.8912	0.8311	0.7979	0.9351	91.89	0.99	91.89±0.11	0.307868
Ensemble	0.9299	0.8389	0.8691	0.861	0.7698	0.7812	0.9365	90.898	0.322	90.898±0.22	0.309534
Experiment 3: Comparing the outcomes of different ML models on selected attributes with minimal cost **0.78808** (PS 15)											
SVM	0.9518	0.8867	0.9125	0.9051	0.8526	0.8527	0.9575	**93.243**	0.3569	**93.243**±0.46	0.311395
RF	0.9427	0.8978	0.8978	0.8978	0.8406	0.8406	**0.9698**	92.664	1.5912	92.664±0.24	0.312395
DT	0.9397	0.8548	0.8882	0.8712	0.8012	0.8015	0.9388	90.926	0.2718	90.926±0.40	0.302541
LR	0.9578	0.8172	0.9156	0.8636	0.7938	0.7967	0.9455	90.733	0.306	90.733±0.22	0.305694
KNN	0.9578	0.8817	0.9213	0.901	0.8475	0.848	0.9652	93.05	1.8182	93.050±0.3968	0.315089
XGBoost	0.9321	0.8901	0.909	0.8999	0.8401	0.853	0.9566	91.44	0.9901	91.44±0.56	0.310965

Table 7 (continued)

Classifier	Specificity	Sensitivity	Precision	F1-score	Kappa score	MCC	AUC value	Accuracy	Execution Time	Standard Deviation	*p*-value (two tailed test)
Ensemble	0.9455	0.891	0.9001	0,9007	0.8375	0.8499	0.9601	92.01	1.009	92.01±0.003	0.312639
Experiment 4: Comparing the outcomes of different ML models on select0.8375ed attributes with minimal cost **0.80926** (PS 20)											
SVM	0.9673	0.8508	0.9333	0.8901	0.8352	0.8372	0.9462	92.664	0.3166	92.664±0.11	0.311251
RF	0.9614	0.895	0.9257	0.9101	0.863	0.8633	**0.9588**	**93.822**	1.4712	**93.822**±0.31	0.312251
DT	0.9762	0.8563	0.9509	0.9011	0.8522	0.8548	0.9451	93.436	0.2434	93.436 ±0.07	0.310726
LR	0.9643	0.8563	0.9281	0.8908	0.8357	0.8372	0.955	92.664	0.3003	92.664±0.11	0.315475
KNN	0.9614	0.8839	0.9248	0.9039	0.8541	0.8546	0.9542	93.436	1.9738	93.436±0.17	0.315475
XGBoost	0.9588	0.871	0.9122	0.8851	0.8477	0.8448	0.9401	92.41	0.6107	92.41±0.21	0.308345
Ensemble	0.9584	0.8618	0.9176	0.8888	0.832	0.8329	0.9435	92.471	0.2721	92.471±0.19	0.309963

Table 8 Table demonstrating most notable results for assessment measures with the fewest features (EPO algorithm)

Minimum number of features	List of features	Highest Specificity (ML model)	Highest Sensitivity (ML model)	Highest Precision (ML model)	Highest F1-score (ML model)	Highest Kappa score (ML model)	Highest Matthews correlation coefficient (MCC) (ML model)	Highest AUC value (ML model)	Highest Accuracy (ML model)	Minimum Execution Time (MET) (ML model)
4	11, 8, 23, 28	0.9940 (LR)	0.8260 (RF)	0.9838 (LR)	0.8811 (RF)	0.8222 (RF)	0.8263 (RF)	0.9516 (RF)	92.084 (RF)	0.3239 (SVM)

Table 9 The highest generated values of different evaluation parameters when EPO FS algorithm is employed. Summing up of best results with FS using EPO. Chart representing the highest results computed for split approach (70:30) with varying population size from 5 to 20

Highest Specificity	Highest Sensitivity	Highest Precision	Highest F1-score	Highest Kappa score	Highest MCC	Highest AUC value	Highest Accuracy	MET
(ML model)	(ML model)	(ML model)	(ML model)	(ML model)	(ML model)	(ML model)	(ML model)	(ML model)
0.9940(LR)	0.8978(RF)	0.9838(LR)	0.9101(RF)	0.8630(RF)	0.8633(RF)	0.9698(RF)	93.822(RF)	0.1119(Ensemble)

Table 10 FS on varying population size (PS) from 5 to 20 implemented splitting approach

Experiment 1: Performance on PS 5						
NoF	NoI	PS		FNo.	FV	ET
36	100	5		2, 4, 15, 17, 29, 35, 36	**0.8104**	5.3794
Experiment 2: Performance on PS 10						
36	200	10	13	2, 4, 8, 16, 18, 21, 22, 24, 27, 29, 31, 32, 35	**0.8542**	24.8557
Experiment 3: Performance on PS 15						
36	200	15	19	2, 3, 5, 7, 8, 10, 11, 13, 15, 16, 19, 20, 21, 24, 26, 29, 31, 32, 33	**0.8239**	49.2316
Experiment 4: Performance on PS 20						
36	400	20	28	1, 2, 3, 4, 5, 6, 8, 9, 13, 14, 15, 16, 17, 18, 19, 20, 21, 22, 24, 25, 26, 27, 28, 29, 32, 34, 35, 36	**0.752**	68.059

properties of the segmented optic disc picture are clinically more relevant in the diagnosis of glaucoma from a fundus image than features of the entire or sub fundus image, according to the experimental findings provided in this work. The suggested method uses the image denoising of digital fundus images to reduce the statistics of the wavelet coefficients of glaucoma photos using a non-Gaussian bivariate probability distribution function. The well-known feature selection procedure was used after the usual visual characteristics were eliminated. The least square support vector machine classifier, which uses a variety of kernel functions, is then given the chosen attributes. This study [21] makes use of the optic disc (OD) and the non-parametric GIST descriptor. Following ground-breaking area-based optic disc segmentation, the radon transformation (RT) is recommended in the methodology. A modified census transformation (MCT) is used to account for differences in the light levels of the radon-converted picture. Using the GIST descriptor, the spatial envelope energy spectrum is then extracted from the MCT pictures. Locality-sensitive discriminant analysis (LSDA) is used to minimize the generated GIST descriptor dimension before utilizing a variety of feature selection and ranking methods. Practitioners provided a unique technique for an automated glaucoma diagnosis using digital fundus pictures in [22]. The iterative Variational Mode Decomposition (VMD) approach was used for picture decomposition. A few of the characteristics that may be derived from VMD components are fractal dimensions, Yager entropy, Renyi entropy, and Kapoor entropy. Following the selection of the discriminating features using the ReliefF approach, the least squares support vector machine (SVM) classifies the data using these features. To automatically identify between normal and glaucoma classes, the approach suggested in the study uses data from higher-order spectra (HOS), trace transforms (TT), and discrete wavelet transforms (DWT) [23]. The SVM classifier performed a exemplary perfromance of differentiating between glaucoma and healthy pictures thanks to its polynomial-order-2 kernel function.

505 fundus photographs were entirely disassembled using quasi-bivariate variational mode decomposition (QB-VMD) [24], resulting in band-limited sub-band images (SBIs) that are tuned to a certain frequency. There are no faults or mode-mixing issues with these SBIs. Using QB-VMD SBIs, 70 features were retrieved. The ReliefF technique is used to choose the retrieved features. The dimension of the selected characteristics is then decreased by feeding them via singular value decomposition. Once the attributes have been decreased, the least square SVM classifier is used to classify them. Glaucoma is recognized using anisotropic dual-tree complex wavelet transform features and a time-invariant

Table 11 Presentation of six ML classifiers performance with varying PS from 5 to 20 with 70:30 approach

Classifiers	Specificity	Sensitivity	Precision	F1-score	Kappa score	MCC	AUC value	Accuracy	Execution Time	Standard Deviation	*p*-value (two tailed test)
Experiment 1: Comparing the outcomes of different ML models on selected attributes with minimal cost 0.81045 and PS5											
L R	0.9646	0.8004	0.9294	0.8588	0.7436	0.7501	0.9561	85.907	0.2495	85.907±1.47	0.310583
Ensemble	0.8888	0.8823	0.9005	0.8784	0.7742	0.7823	0.9602	88.999	0.2635	88.999±0.09	0.312543
DT	0.9324	0.8164	0.8894	0.8513	0.7593	0.7611	0.9582	88.61	0.2495	88.610±0.46	0.311586
SVM	0.9389	0.8647	0.904	0.8095	0.8095	0.81	0.9613	90.926	0.3153	90.926±0.413	0.313071
KNN	0.9421	0.8405	0.9062	0.8721	0.7923	0.7937	0.96	90.154	1.4333	90.154±0.413	0.312447
RF	0.9614	0.8647	0.9371	0.8994	0.8369	0.8387	**0.9701**	**92.277**	1.5283	**92.277** ±0.92	0.313447
XGBoost	0.9521	0.854	0.8999	0.87	0.793	0.7809	0.9641	91.98	1.0009	91.98±0.81	0.314416
Experiment 2: Comparing the outcomes of different ML models on selected attributes with minimal cost 0.85425 and PS 10											
LR	0.9654	0.875	0.9408	0.9067	0.8514	0.8528	0.9661	93.05	0.321	93.050±0.01	0.31044
KNN	0.9591	0.919	0.9333	0.9215	0.8731	0.8733	0.968	94.015	2.7253	94.015±0.35	0.311347
DT	0.9245	0.905	0.8829	0.8938	0.8256	0.8258	0.9531	91.698	0.275	91.698±0.50	0.304279
RF	0.9748	0.895	0.9572	0.8804	0.8804	0.8817	**0.9804**	**94.401**	1.9002	94.401±0.48	0.314279
SVM	0.9591	0.912	0.9333	0.9215	0.8731	0.8733	0.9642	94.015	0.459	94.015±0.48	0.304279
XGBoost	0.9461	0.901	0.8967	0.8906	0.8577	0.8632	0.9551	92.45	0.9221	92.45±0.22	0.305222
Ensemble	0.949	0.888	0.9123	0.8999	0.8301	0.859	0.966	91.999	0.32	91.999±0.40	0.310392
Experiment 3: Comparing the outcomes of different ML models on selected attributes with minimal cost 0.82395 and PS 15											
SVM	0.9693	0.8385	0.9415	0.887	0.8264	0.8297	0.9322	92.0849	0.4286	92.0849±.44	0.309249
RF	0.9846	0.9218	0.9725	0.9465	0.9163	0.9171	**0.949**	**96.1389**	2.0286	**96.1389**±1.11	0.319249
DT	0.9509	0.901	0.9153	0.9081	0.8547	0.8547	0.908	93.2432	0.4291	93.2432±0.022	0.297876
LR	0.9723	0.8645	0.9485	0.9046	0.8524	0.8546	0.9371	90.9324	0.369	90.9324±0.85	0.311586
KNN	0.9723	0.8757	0.9491	0.9105	0.8612	0.8629	0.9402	93.629	2.7743	93.629±0.14	0.313071
XGBoost	0.95	0.896	0.9311	0.8998	0.8543	0.8484	0.9376	92.7712	0.8877	92.7712±0.14	0.311825
Ensemble	0.9601	0.899	0.9299	0.9095	0.8601	0.8612	0.9422	93.4701	0.4349	93.4701±0.10	0.314031

Table 11 (continued)

Classifiers	Specificity	Sensitivity	Precision	F1-score	Kappa score	MCC	AUC value	Accuracy	Execution Time	Standard Deviation	*p*-value (two tailed test)
Experiment 4: Comparing the outcomes of different ML models on selected attributes with minimal cost 0.75206 and PS 20											
SVM	0.9695	0.8842	0.9438	0.913	0.8652	0.8663	0.9562	93.822	0.3855	93.822±0.06	0.310153
RF	0.9786	0.8842	0.96	0.9205	0.8774	0.8792	**0.9711**	**94.401**	2.0934	**94.401**±0.28	0.311153
DT	0.9664	0.9	0.9395	0.9193	0.8742	0.8746	0.9461	94.208	0.407	94.208±0.20	0.305363
LR	0.9786	0.8631	0.959	0.9085	0.8599	0.8627	0.9629	93.629	0.3706	93.629±0.01	0.313358
KNN	0.9695	0.8684	0.9428	0.9041	0.852	0.8538	0.9533	93.243	2.6188	93.243±0.14	0.308773
XGBoost	0.9701	0.8677	0.9432	0.8998	0.8412	0.851	0.9455	93.21	0.879	93.21±0.14	0.30508
Ensemble	0.9756	0.8726	0.9529	0.9	0.8469	0.85	0.9499	93.05	0.4855	93.050±0.22	0.30716

Table 12 Table showing the optimal performance metrics with the fewest characteristics used during BFO deployment

Minimum features extracted	List of features	Highest Specificity (ML model)	Highest Sensitivity (ML model)	Highest Precision (ML model)	Highest F1-score (ML model)	Highest Kappa score (ML model)	Highest MCC (ML model)	Highest AUC value (ML model)	Highest Accuracy (ML model)	MET (ML model)
7	2, 4, 15, 17, 29, 35, 36	0.9646 (LR)	0.8840 (Ensemble)	0.9371 (RF)	0.8994 (RF)	0.8369 (RF)	0.8387 (RF)	0.9531 (RF)	92.277 (RF)	0.2495 (LR, DT)

Table 13 The peak values of different indicators produced using BFO algorithm. A comprehensive overview of feature selection with the BFO algorithm. The best results for split approach (70:30) with different population sizes (5, 10, 15 and 20) are presented in the table

Highest Specificity (ML model)	Highest Sensitivity (ML model)	Highest Precision (ML model)	Highest F1-score (ML model)	Highest Kappa score (ML model)	Highest MCC (ML model)	Highest AUC value (ML model)	Highest Accuracy (ML model)	MET (ML model)
0.9846(RF)	0.9218(RF)	0.9725(RF)	0.9465(RF)	0.9163(RF)	0.9171(RF)	0.9804(RF)	96.1389(RF)	0.2495 (LR, DT)

Table 14 FS on PS 5 , 10, 15 and 20 for splitting approach

Experiment 1: Performance on PS 5						
NoF	NoI	PS	FSel	FNo.	FV	ET
36	400	5	8	1, 8, 13, 14, 15, 19, 21, 28	**0.8186**	2.2669
Experiment 2: Performance on PS 10						
36	400	10	16	1, 2, 3, 4, 5, 13, 14, 20, 21, 23, 25, 26, 27, 31, 32, 34	**0.8807**	6.4523
Experiment 3: Performance on PS 15						
36	300	15	20	1, 4, 9, 11, 13, 14, 15, 18, 20, 21, 22, 23, 24, 25, 26, 28, 30, 31, 32, 36	**0.7683**	10.6695
Experiment 4: Performance on PS 20						
36	400	20	23	1, 2, 3, 4, 5, 7, 10, 11, 12, 13, 14, 15, 16, 17, 18, 19, 20, 22, 23, 24, 28, 33, 35	**0.8346**	16.0964

cup-to-disc (CDR) ratio [25]. Fuzzy C-Means clustering was used to segment the optic disc, while Otsu's thresholding was employed to segment the optic cup. Fundus pictures were used in this study's Cup to Disc Ratio (CDR) measurement in order to identify glaucoma [26]. Using Au-Net, the borders of OD and optic cup (OC) were segmented throughout the feature extraction process. The glaucomatous images were then reduced using a random forest classifier based on the CDR values. Deformable, full-deformable, and original U-Nets have all been used to test the success of the suggested course of action. The extraction of GIST and pyramid histogram of oriented gradients (PHOG) features from preprocessed fundus pictures was the main emphasis of this paper [27]. Principal component analysis (PCA) was used to filter and pick the most important attributes from the obtained features, which were then sent to an SVM classifier for classification.

This research, [28], provides a mathematical technique combined with region-based deep convolutional neural networks to provide a reliable and effective optic disk detection and fovea localization method. There are two phases to the suggested model: Using Faster R-CNN, the authors initially created a number of optic disk region proposals before identifying the optic disk by utilizing the boundary box with the greatest score. Using a mathematical model and the coordinates of the anticipated optic disk region, they determined the localization of the fovea in the second stage. The cuckoo search algorithm and structural similarity index measure are used to localize the optic disk in retinal images in this paper [29]. Average optic disk is compared to candidate optic disk by SSIM. Randomly selected images were used to calculate average optic disk values. The algorithm used average optic disk values and colored retina fundus images. To match brightness and contrast across images, adaptive histogram equalization was used. Next, the search algorithm calculated candidate optic disk centers and calculated their similarity to the average optic disk. The search algorithm found the true optic disk center by maximizing computed similarity.

Weakly-Supervised Concealed Object Segmentation (WSCOS) trains models with sparsely annotated data to separate objects well integrated into their contexts [30]. Intrinsic similarity makes it hard to distinguish hidden items from the background, and sparsely labelled training data provide insufficient supervision for model learning. Authors address these two issues with a new WSCOS approach in the work. A multi-scale feature grouping module aggregates results from multiple granularities to solve the intrinsic similarity problem. Grouping related features improves segmentation coherence, resulting in complete single- and multi-object segmentation. They build segmentation masks for model

Table 15 Evaluation of implemented ML classifiers on varying PS 5 to 20 with a gap of 5 (70:30 Splitting Approach)

Classifiers	specificity	sensitivity	precision	F1-score	Kappa score	MCC	AUC value	Accuracy	Execution Time	Standard Deviation	p-value (two tailed test)
Experiment 1: Comparing the outcomes of different ML models on selected attributes with minimal cost 0.81865 (PS5)											
LR	0.979	0.8043	0.9548	0.8731	0.8121	0.8187	0.9557	91.698	0.4911	91.698±0.28	0.310297
RF	0.9401	0.9076	0.893	0.9002	0.8446	0.8447	**0.9703**	92.857	1.3155	92.857±0.14	0.320297
DT	0.9161	0.9347	0.8799	0.8958	0.8346	0.8364	0.9581	92.277	0.2536	92.277±0.06	0.311442
SVM	0.991	0.8043	0.9801	0.8835	0.8287	0.8375	0.961	92.471	0.3447	92.471±0.01	0.312831
KNN	0.97	0.8641	0.9408	0.9008	0.8497	0.8515	0.96	**93.243**	2.5486	**93.243**±0.29	0.312352
XGBoost	0.9595	0.8899	0.9351	0.8989	0.8373	0.8388	0.958	92.1	0.8881	92.100±0.13	0.311395
Ensemble	0.96	0.901	0.941	0.8999	0.841	0.842	0.9601	92.555	0.9931	0.9931±0.03	0.312399
Experiment 2: Comparing the outcomes of different ML models on selected attributes with minimal cost 0.88075 (PS 10)											
SVM	0.9657	0.8934	0.9411	0.9166	0.8676	0.8683	0.9644	93.822	0.2947	93.822±0.26	0.309868
RF	0.9937	0.8934	0.9887	0.9386	0.904	0.9068	**0.9799**	**96.559**	1.4688	**96.559**±0.76	0.319868
DT	0.9781	0.8984	0.9619	0.9291	0.8879	0.8892	0.9534	94.787	0.2021	94.787±0.08	0.304656
LR	0.9813	0.8883	0.9668	0.9259	0.8834	0.8854	0.9662	94.594	0.2647	94.594±0.01	0.310726
KNN	0.9781	0.8832	0.9613	0.9206	0.8751	0.8771	0.9675	94.208	2.1612	94.208±0.01	0.311347
XGBoost	0.9654	0.8801	0.9312	0.9143	0.8872	0.8738	0.9601	93.991	1.0234	93.991±0.20	0.307823
Ensemble	0.9701	0.8809	0.9492	0.9276	0.8845	0.8862	0.9664	93.887	0.253	93.887±0.64	0.310821
Experiment 3: Comparing the outcomes of different ML models on selected attributes with minimal cost 0.76834 (PS 15)											
SVM	0.9582	0.8469	0.9171	0.8806	0.8194	0.8209	0.9322	91.891	0.3611	91.891±0.29	0.309296
RF	0.9611	0.8524	0.923	0.8863	0.828	0.8295	**0.9489**	**92.277**	1.8088	**92.277**±0.43	0.319296
DT	0.9343	0.8142	0.8713	0.8418	0.7598	0.7608	0.9078	89.189	0.2688	89.189±0.72	0.297458
L R	0.9522	0.8306	0.9047	0.866	0.7976	0.7993	0.937	90.926	0.4141	90.926±0.06	0.311586
KNN	0.9582	0.8251	0.9151	0.8678	0.8012	0.8036	0.9396	91.119	2.5092	91.119±0.017	0.312831
XGBoost	0.9456	0.8578	0.8923	0.8688	0.8009	0.793	0.9379	90.99	0.6331	90.990±0.083	0.312016
Ensemble	0.9501	0.8601	0.8991	0.8741	0.8001	0.7999	0.9422	91.333	0.9999	91.333±0.08	0.314079

Table 15 (continued)

Classifiers	specificity	sensitivity	precision	F1-score	Kappa score	MCC	AUC value	Accuracy	Execution Time	Standard Deviation	p-value (two tailed test)
Experiment 4: Comparing the outcomes of different ML models on selected attributes with minimal cost 0.83461 (PS 20)											
SVM	0.9723	0.8958	0.9502	0.9222	0.8785	0.8795	0.9563	**94.401**	0.3476	**94.401**±0.27	0.310487
RF	0.9723	0.8802	0.9494	0.9135	0.8655	0.867	**0.9705**	93.822	1.901	93.822 ±0.06	0.320487
DT	0.957	0.8854	0.9239	0.9042	0.8497	0.8502	0.946	93.05	0.2802	93.050±0.22	0.305599
LR	0.9693	0.8854	0.9444	0.9139	0.8658	0.8669	0.9634	93.822	0.313	93.822±0.16	0.313887
KNN	0.9693	0.8697	0.9435	0.9051	0.8528	0.8545	0.9532	93.243	2.5271	93.243±0.14	0.309011
XGBoost	0.9797	0.8762	0.9501	0.9088	0.8612	0.8701	0.9488	93.119	0.999	93.119±0.20	0.306923
Ensemble	0.9805	0.8845	0.9689	0.9177	0.87	0.8787	0.9503	94.231	0.3188	94.231±0.21	0.307634

Table 16 A table with the hybrid algorithm's best performance measurements when it picked the fewest features

Minimum features extracted	List of features	Highest Specificity (ML model)	Highest Sensitivity (ML model)	Highest Precision (ML model)	Highest F1-score (ML model)	Highest Kappa score (ML model)	Highest MCC (ML model)	Highest AUC value (ML model)	Highest Accuracy (ML model)	MET (ML model)
8	1, 8, 13, 14, 15, 19, 21, 28	0.9910 (SVM)	0.9347 (DT)	0.9801 (SVM)	0.9008 (KNN)	0.8497 (KNN)	0.8515 (KNN)	0.9703 (RF)	93.243 (KNN)	0.2536 (DT)

Table 17 The highest values of different metrics computed from the features returned by hybrid algorithm. A comprehensive overview of the results produced using hybrid algorithm for feature selection. The table shows the highest results of various metrics with PS 5 to 20 with variation of 5 during split approach implementation

Highest Specificity (ML model)	Highest Sensitivity (ML model)	Highest Precision (ML model)	Highest F1-score (ML model)	Highest Kappa score (ML model)	Highest MCC (ML model)	Highest AUC value (ML model)	Highest Accuracy (ML model)	MET (ML model)
0.9910(SVM)	0.9347 (DT)	0.9887(RF)	0.9386(RF)	0.9040(RF)	0.9068(RF)	0.9799(RF)	96.559(RF)	0.2021(DT)

Table 18 The highest values of different metrics in three cases

Highest Specificity (ML model)	Highest Sensitivity (ML model)	Highest Precision (ML model)	Highest F1-score (ML model)	Highest Kappa score (ML model)	Highest MCC (ML model)	Highest AUC value (ML model)	Highest Accuracy (ML model)	MET (ML model)
Case-I Best results produced by the proposed approach when tested on **customized** dataset								
0.9940(SVM)	0.9347 (DT)	0.9887(RF)	0.9386(RF)	0.9163(RF)	0.9171(RF)	0.9804(RF)	96.559(RF)	0.2021(DT)
Case-II Best results produced by the proposed approach when tested on **In-house(private)** dataset								
0.9959(SVM)	0.9512 (RF)	0.9901(DT)	0.9452(RF)	0.9199(RF)	0.9287(RF)	0.9888(RF)	97.437(RF)	0.2999(DT)
Case-III Best results produced by the proposed approach when tested on **public** dataset								
0.9910(SVM)	0.9289(DT)	0.9728(RF)	0.9279(RF)	0.9003(RF)	0.9034(RF)	0.9743(RF)	95.789(RF)	0.3159(SVM)

Table 19 Evaluating the effectiveness of a proposed novel approach in contrast to previous work

Study	Classification method	Dataset and/or No. of images	Accuracy	Sensitivity	Specificity
Guo et al. [75]	ML	ORIGA	76.90	0.799	0.738
Liu et al. [76]	DL	650 images of ORIGA dataset and 400 images from REFUGE dataset.	ORIGA (76.57) REFUGE (82.78)	ORIGA (0.7273) REFUGE (0.7)	ORIGA (0.8041) REFUGE (0.956)
Fu et al. [77]	DL	ORIGA ,Singapore Chinese Eye Study and the third dataset is a population-based study conducted	84.29	0.8478	0.8380
Martins et al. [46]	DL	2482 images from ORIGA and other datasets	88	0.83	0.90
Sreng et al. [78]	11 DL models, then SVM and finally their ensemble.	2787 images from REFUGE, ACRIMA, ORIGA and other datasets	From 80.00 (ORIGA) to 95.59 (REFUGE)	Not Reported	Not Reported
Orlando et al.[79]	DL	REFUGE	Not Reported	0.9752	Not Reported
Guo et al. [80]	Gradient boosting decision tree (GBDT)	650 images of ORIGA	84.3	0.894	0.793
Abad et al. [81]	DL	10658 images from REFUGE, and other datasets	95.3	0.841	0.958
Elangovan[82]	DL	ORIGA	78.32	0.5806	0.9244
Tulsani et al. [83]	DL	650 images of ORIGA	90	0.87	0.81
Juneja et al. [84]	DL	DRISHTI –DS	95.03	0.7379	0.8623
Jerith and Kumar[63]	Feature selection through gray wolf algorithm	Not Reported	93.103	0.916777	0.94117
Kirar et al. [85]	DWT and LS-SVM	505 images of RIM-1 dataset	84.95	0.86	0.8385
Parashar and Agrawal[47]	Feature Selection and SVM classifier	A total of 941 images representing the RIM-ONE, ORIGA, DRISHTI, and HRF datasets.	90.76	0.945	0.8784
Gour & Khanna[27]	GIST and PHOG descriptors	A total of 60 images of HRF were obtained, with the remaining images sourced from the Drishti GS dataset.	83.4	Not Reported	Not Reported

Table 19 (continued)

Study	Classification method	Dataset and/or No. of images	Accuracy	Sensitivity	Specificity
Singh et al. [7]	Combination of metaheuristic algorithm (Gravitational search optimization algorithm) for FS)) and ML techniques (for classification)	Self-Customized dataset of more than 3000 images	Upto 95.30	Upto 0.917	Upto 0.996
Singh et al. [34]	Combination of metaheuristic algorithm (for FS)) and ML techniques (for classification)	ORIGA	Upto 96.80	Upto 0.992	Upto 0.901
Singh et al. [86]	Combination of statistical approaches with metaheuristic algorithm (for FS)) and ML techniques (for classification)	DRIONS-DB	Upto 99.00	Upto 0.970	Upto 0.960
Singh et al. [87]	Multimodal features fusion and Image fusion approach with late fusion of results and ML techniques (for classification)	2555 images (Combination of (REFUGE, ORIGA, and ACRIMA)	Upto 95.96	Upto 0.920	Upto 0.960
Singh et al. [88]	Combination of metaheuristic algorithm (for FS)) and ML techniques (for classification)	2 Public Datasets (ORIGA and REFUGE) Upto 1850	Upto 98.9524	Upto 0.9808	Upto 0.9481
Proposed method	Nature inspired computing and machine learning approaches	A total of 3112 images were obtained through the amalgamation of publicly available datasets and privately sourced images.	Upto 96.55	Upto 0.9347	Upto 0.9940

training using the recently proposed vision foundation model, Segment Anything Model (SAM), and sparse annotations for the weak supervision challenge. Multi-augmentation result ensemble, entropy-based pixel-level weighting, and image-level selection can reduce low-quality segmentation masks. They enhance segmentation model training supervision. Authors find our method works well on several WSCOS jobs. Camouflaged object detection (COD) works to identify items visually blended into their surroundings. Camouflaged objects' background resemblance and unclear borders make COD difficult [31]. There are several ways to mimic the human visual system. Although disguised objects deceive the vision system, these strategies work in many situations. Researchers propose the COD FEature Decomposition and Edge Reconstruction (FEDER) model. The FEDER model addresses foreground-background similarities by decomposing features into frequency bands using learnable wavelets. Small foreground-background hints from the most informative bands are mined. Create frequency attention and guidance-based feature aggregation modules. The recommend learning COD and an auxiliary edge reconstruction task to solve the ambiguous boundary problem. Authors ODE-based edge reconstruction tool creates accurate edges. By learning the auxiliary task with the COD task, the FEDER model can create accurate object boundary prediction maps.

Unpaired medical image enhancement (UMIE) improves LQ medical images to HQ without paired images [32]. Most effective systems use Pix2Pix/Cycle GAN, but they don't explicitly use HQ information to drive the augmentation process, which may cause artefacts and structural distortions. This research proposes a novel UMIE method that directly encodes HQ cues into the LQ enhancement process in a variational form to simulate the UMIE problem under the combined distribution of the LQ and HQ domains, avoiding the limitations of existing methods. To guide LQ enhancement with the variational normalization module, we explicitly integrate HQ picture characteristics into the enhancement network. Their purpose is to encode HQ cues. To ensure HQ image, we train the enhancement network adversarially with a discriminator. Authors proposed content-aware loss, wavelet-based pixel-level, and multiencoder-based feature-level constraints for enhancement. A bi-level learning scheme to optimize the UMIE task and downstream tasks cooperatively to generate visually appealing and suitable HQ images is proposed to improve downstream tasks. Three medical datasets demonstrate that the suggested strategy improves quality and job performance better than existing methods. Camouflaged object detectors (COD) involve spotting camouflaged items in the environment. In difficult situations, COD detectors still give inaccurate readings despite their popularity [33]. Researchers designed algorithms for both sides based on the prey-vs-predator game, which improves prey camouflage and predator vision. Camouflageator, an adversarial prey training framework, generates more camouflaged items that COD methods cannot detect using an auxiliary generator. Adversarial camouflageators teach the generator and detector, strengthening the detector with a stronger auxiliary generator. A predator-side COD approach called Internal Coherence and Edge Guidance (ICEG) extracts camouflaged objects' internal coherence using a disguised feature coherence module for better segmentation. ICEG suggests an edge-guided segregated calibration module to avoid inaccurate predictions and unclear bounds. ICEG outperforms conventional COD detectors in numerous trials, and Camouflageator can improve any COD detector to state-of-the-art performance.

The Grey Wolf Optimizer (GWO) and Whale Optimization Algorithm (WOA) are used in this empirical study to create a novel and effective methodology [34]. As novel, innovative scientific contribution, authors created the hybrid version (hGWWO) of these two approaches. The baseline algorithms above have been used for feature selection across domains. These three algorithms are being used for the first time to identify glaucoma,

especially on the public benchmark dataset ORIGA. Classifying fundus retinal images under investigation uses nature-inspired computing strategies for feature selection and ML models for classification. The ORIGA dataset yielded 65 features. Three soft-computing-based feature selection methods select the most influential features from the dataset. Machine Learning classifiers are trained on this data and evaluated 70:30. Ophthalmologists can use the deep learning system to diagnose glaucoma fundus lesions like retinal nerve fiber layer defects, optic nerve head damage, and optic disc hemorrhage [35]. Early detection of these lesions can prevent structural damage, visual function loss, and visual field damage. Deep convolutional neural networks, developed from deep learning, are integrating artificial intelligence with testing devices like visual field meters, fundus imaging, and optical coherence to accelerate clinical glaucoma diagnosis and prediction. Some of the advances in glaucoma diagnosis and prediction using artificial intelligence, visual field, fundus photography, and optical coherence tomography are familiar—some are not. Then authors discuss current challenges and future clinical applications.

Temporal data carpentry and machine learning and logistic regression methods were used to create a predictive analytic framework for early glaucoma prediction using EHR from over 650 US hospitals and clinics [36]. The entire dataset was predictively analyzed using four machine-learning classification methods. Five-fold cross-validation trained and refined models to calculate accuracy, sensitivity, specificity, and f1 score. Compared to logistic regression (LR) at 0.73, XGBoost, MLP, and RF performed similarly well in predicting glaucoma one year before its onset with AUC scores of 0.81 and 0.73, respectively. Machine learning (ML) model performance improvement depends on FS, which selects the most influential subset of features. Researchers recommended metaheuristic-based FS using the Gravitational search optimization algorithm (GSOA) [7]. Optic nerve fibers can degrade and cannot be replaced in this disease. Starting with retinal fundus images of glaucoma patients and healthy people, 36 features were retrieved from public benchmark datasets and private datasets. The approach used the GSOA's returned subset of features to train six ML models for classification. Selecting key features improves classification performance with the suggested FS method. The eight statistical performance parameters and execution time are calculated. The training and testing used a split approach (70:30), 5-fold CV, and 10-fold CV. The suggested method was 95.36% accurate in classification task. This study uses fewer structural and nonstructural features to characterize retinal fundus images[37]. Authors extracted the grey level co-occurrence matrix (GLCM), grey level run length matrix (GLRM), first order statistical matrix (FOS), wavelet, and structural features like DDLS and CDR. The set of features was sent to three classical nature inspired algorithms (Particle Swarm Optimization (PSO), Artificial Bee Colony (ABC), and Binary Cuckoo Search (BCS)) and their two-layered model (PSO-ABC) to generate a subset of reduced features (feature selection phase) that computes auspicious accuracy when sent to three ML classifiers. Researchers believe these four soft computing algorithms are rarely used in this application. Subject datasets ORIGA, REFUGE, and their combinations are used to evaluate suggested strategy. Calculations include accuracy, specificity, precision, and sensitivity. The BCS performs well with 91% to 98.46% accuracy. With minor accuracy loss, PSO-ABC greatly reduces the feature set.

It has proven possible to sort super-pixels for glaucoma screening utilizing histograms and center-surround data (Cheng et al [38]). Kolar and Jan [39] integrated an SVM with power spectral features and fractal dimensions (FDs). Singh et al. [40] employed various deep learning models for performance evaluation investigation on different glaucoma benchmark datasets. Higher-order spectra and complex wavelet transform were used by Raja and Gangatharan [41]. Along with entropy and energy maps, they used wavelet packet

decomposition (WPD) as a characteristic. Kirar and Agrawal have suggested the DWT and histogram functions for this infection identification [42]. Kirar and Agrawal [43] recommended the use of 2D-DWT to distinguish between images showing glaucoma and images of unaffected eyes, and histogram-based characteristics were used to carry out the classification. Yadav et al. used glaucoma fundus images for texture-based feature extraction and categorization [44]. Empirical wavelet transform (EWT) was employed by Maheshwari et al. [45] to disassemble fundus images. In the recently released study on glaucoma diagnosis utilizing fundus images [46, 47], it has been shown that the least square-SVM was helpful for using on fundus pictures in two categories.

A comparative table (Table 1) is shown below, in which we have discussed 25 state-of-the-art studies published on glaucoma identification through feature extraction, followed by feature selection, and then finally image classification.

Most of the research discussed in Table 1 has primarily concentrated on feature selection using a variety of techniques, which is necessary for the disease's confirmation. While some authors [48, 50, 51] have concentrated on the HOS features, other have focused on features like wavelet features [20, 49, 55, 58, 60, 68], textural [48], geostatistical [57], statistical [59], HOG [63], GLCM [63, 66], wavelet [55], and Gabor filters [52, 55]. Some researchers have shifted their focus to extracting structural features from subject retinal fundus images [53–56, 62, 67, 69]. Principal component analysis (PCA), linear discriminant analysis (LDA), independent component analysis (ICA), singular value decomposition, T-test, Bhattacharyya distance method, entropy ranking method, gain ratio, co-relation, relief feature ranking, neighborhood component analysis, sequential floating forward selection method, and Wilcoxon rank-sum test method are some of the approaches used for subset construction of the most informative features after feature extraction. Additionally, it was observed that fewer studies—some of which used genetic algorithms and particle swarm intelligence—have been published that use nature-inspired computing techniques for feature selection. In order to introduce a novel and effective feature selection approach, the current study has innovated by utilizing two recently developed nature-inspired computing algorithms along with their hybridized versions. The most demanding classifiers identified from above table for classification were SVM and its variants (such as TWIN SVM and Least Squares SVM). Neural networks, multi-layer perceptrons, KNNs, and RF have been used by others. Nonetheless, seven machine learning classifiers are used in this empirical study to identify the nine statistical performance measuring metrics that plays the key role. These earlier studies used benchmark datasets that differ significantly from one another. The studies listed in Table 1 each work separately on these datasets, but the current study looks into how these datasets are combined to create one of the largest datasets.

After a thorough examination of this table, which contains 25 cutting-edge studies, we have determined that researchers are continuously and assiduously pursuing novel approaches for the early and prompt screening of this disease. In each of these investigations, multiple image processing-based features are extracted from the fundus. However, in the majority of these studies, as indicated above, the feature extraction is limited to one, or two classes of features, however our work is more improved to almost all in this term because we have extracted more than two classes of features.

In our case, the extracted features are then cut down to make a subset of them that works very well and can be highly trusted. This operation is carried out in virtually all research, utilizing various mathematical or statistical methods. Only one or two studies have used nature inspired computing-based classical methodologies such as genetic algorithms (GA) or particle swarm optimization (PSO) for feature selection; this is one of the most significant research gaps we have uncovered. GA and PSO are classically old algorithms with

their own problems, which is why academics are developing novel nature inspired computing algorithms, such as BFO and EPO. This motivated us to select these feature-picking methods. In addition, we've applied a third algorithm that is a hybrid combination of these two, which we've proposed. On the basis of this table and our review of the relevant literature, we can confidently assert that we are the ahead in applying three nature inspired-computing-based methods for efficient and robust feature selection for early, efficient and timely glaucoma identification. The suggested technique's performance is evaluated using commonly recognized benchmark fundus images. The methodology presented in this study is utilized to determine the most suitable combination of attributes, with the primary aim of improving the accuracy of classification while simultaneously minimizing the selection of features and error rate. The utilization of both well-defined and hybrid data transformation algorithms leads to the production of the most optimal subset of features from a range of benchmark datasets.

2.1 Research gap identification and Justification of the proposed approach

Data mining is a potent new method for extracting data warehouse secrets. Data mining analyses enormous amounts of raw data to identify patterns and knowledge. Data mining approaches like clustering and classification are useful in banking, supply chain management, insurance, vehicular ad hoc networks, and wireless sensor networks. Medical researchers have used data mining to investigate genetic and environmental disease agents and improve diagnostic tools for many patients. Researchers gain insight into the environmental and genetic causes of diseases and develop more effective diagnostic procedures by mining vast datasets of patients. Data storage has expanded due to the rapid growth of the internet, IoT, and RFID. Given the expanding amount of data processed by application systems integrated inside devices that are internet-accessible, saving the data is essential. Clearing and extracting appropriate information and feature selection approaches are becoming more critical. Feature selection decreases running time by eliminating unnecessary and redundant information, boosting classification accuracy, and simplifying learnt classifiers or models. With several features, feature selection is difficult. Complex categorization problems involve several features. Thus, the classifier classifies observations across time.

Medical research and diagnostics depend on finding effective illness detection features. Despite advances in machine learning and medical imaging, research gaps remain. Gaps include:

Feature Selection and Extraction: Finding the best medical data features for disease detection is difficult. More advanced algorithms are needed to extract discriminative characteristics from complicated and diverse datasets, notably in medical imaging like MRI, CT, and histopathology images.
Interpretability of traits: Machine learning models may discover traits as important for disease detection, but interpreting their biological or clinical relevance is difficult. To close this gap, models must accurately forecast diseases and explain selected traits in a clinically interpretable manner.

Medical datasets often have small sample sizes for rare diseases or uneven distributions across disease classes. This hinders accurate and generalizable model training. We need

methods to handle short sample numbers and class imbalances while preserving model performance.

Features are selected to minimize dataset dimensionality, enhance classification accuracy, and prevent overfitting to increase wireless sensor network efficiency and energy consumption and lengthen network lifetime. The main challenge in feature selection difficulties is discarding some of the pre-processed data without affecting quality. Many methods have been developed for feature selection. These algorithms had a hefty computing cost when they were introduced 30 years ago. This challenge was solved by fast computers and large storage resources, but creating a fast solution to deliver this function is still relevant due to new challenges' enormous data sets. Compressive sensing technology has been presented by many academics to eliminate data redundancy and limit the number of nodes in wireless sensor networks to save energy consumption. The above method samples fewer points than needed for signal capture and reconstruction with high probability. New and efficient optimization methods include evolutionary game theory, graph theory, and heuristics. Optimization methods can be divided into exact and approximate algorithms. Exact algorithms can optimize exactly but are inefficient in robust optimization and take exponentially longer to solve. Close to optimization, approximate techniques can solve robust optimization issues quickly. Heuristic and metaheuristic approximate algorithms exist. Q-learning algorithm identifies limited search space and produces high-quality results in reasonable computation times. They are employed in many commercial packages because they can easily face real-world limits. Evolutionary algorithms help solve mobile ad hoc networks, quantitative association rules, and traveling salesman problems. A feature selection procedure begins with an exhaustive search through the subset of features to find the best feature among the primary probable subclasses based on a given assessment criterion. If the feature set has n features, the best subset must be selected using optimum feature selection. Since evolutionary computation approaches provide global search, they are used as a strong solution and alternative to standard searching methods to handle these challenges. Particle swarm optimization, genetic algorithms, genetic programming, and ant colony optimization are popular feature selection methods. Heuristic models use diverse tactics to find the tradeoff between exploration and exploitation. Exploration helps uncover clear search spaces, whereas exploitation helps maintain better solutions by examining the local search space. Some meta-heuristic search methods use exploration, while others use exploitation for superior results. Using hybrid approaches can improve search algorithm performance. The yield of each approach increases when hybridization combines positive qualities of at least two procedures. This study uses BFO and EPO, two novel and effective meta-heuristics, to construct a hybrid strategy to improve general categorization tasks. This research presented a hybrid feature selection approach using filter and wrapper methods. This model aims to simplify moderate-dimensional feature selection computations.

Wrapper techniques are computationally complex since they select a feature subset and run the classifier on it each iteration, then compute classification accuracy from the confusion matrix. Integration of the filter and wrapper methodologies uses the speed and power of filter and wrapper techniques to identify relevant dataset features. A combination of classification techniques, BFO algorithm, EPO algorithm, and their hybrid was utilized to extract dataset features. Integrating these two algorithms' balances exploration and exploitation to develop an algorithm without the previous flaw by exploiting their strengths—high convergence speed and exploration ability. Only features with a selection probability matching the final subset are expected to align with classification, and the feature

selection procedure is only applied to these. According to several writers, prediction methods are effective for achieving good results. So, the algorithm's computational complexity is reduced and a subset with fewer features is chosen. The suggested approach accelerates feature selection for high-dimensional datasets, improves classification accuracy, and reduces feature selection. By comparing this approach on our unique mid-dimension dataset, this research shows its success. Therefore, the current study goal is to address the question. Will combining the BFO and EPO algorithms in the proposed approach's evaluation function pick influential characteristics and improve classification accuracy also.

3 Materials and methods

This section gives important information on the three-nature inspired computing-based FS techniques that were employed and focuses on the datasets that were chosen for this experimental study.

3.1 Dataset

The dataset utilized in this study comprises a fusion of images sourced from five widely recognized benchmark public datasets, alongside a proprietary dataset procured from hospitals situated in close proximity. The analysis involved a dataset consisting of 3112 images, of which 1226 were categorized as glaucomatic and 1886 were categorized as healthy. A diverse range of sources, including ACRIMA, DRISHTI, HRF, ORIGA, and a privately-owned dataset, were utilized to obtain a comprehensive collection of 3112 images. The ACRIMA dataset comprised 396 images depicting glaucomatous eyes and 309 images representing healthy eyes. Furthermore, the DRISHTI dataset made a valuable contribution by providing a total of 16 images depicting eyes affected by glaucoma. The Human Retinal Fundus (HRF) dataset consisted of a collection of 30 images. Among these images, 15 of them portrayed glaucomatous conditions while the remaining 15 images depicted healthy conditions. In contrast, ORIGA made a substantial contribution by providing a more extensive dataset comprising 650 images. Among these, 168 images exhibited glaucomatous conditions, while the remaining 482 images portrayed healthy conditions. Furthermore, the private dataset consisted of a total of 631 images illustrating glaucomatous conditions and 1080 images depicting healthy conditions (Table 2).

The images in the ACRIMA database are from the ACRIMA project (TIN2013-46751-R), which was started by Spain's Ministerio de Economía y Competitividad with the goal of creating automatic algorithms for the evaluation of retinal diseases. There are 705 fundus images in the ACRIMA database (396 glaucomatous and 309 normal images). They were taken from glaucomatous and normal patients with their prior agreement and in compliance with the ethical guidelines outlined in the 1964 Declaration of Helsinki as part of the ACRIMA research. Experts chose each patient based on their criteria and the clinical results of the test. The majority of the fundus photos in this collection came from the right and left eyes, which had previously been dilated and positioned in the optic disc. A few of them were eliminated due to noise, artifacts, and inadequate contrast. The IMAGEnet® capture system and the Topcon TRC retinal camera were used to record them. Photographs were captured using a 35° field of view. Two eight-year-old glaucoma specialists annotated

every picture from the ACRIMA database. When assigning labels to the photos, no additional clinical data was used. The ACRIMA database's initial iteration was limited to categorization tasks.

With a FOV of 30 degrees, the Drishti collection consists of many retinal fundus images. The photos have a resolution of 2896 x 1944 pixels and are saved as uncompressed PNG files. The Aravind Eye Hospital in India provided the images used in this collection. The age range of the chosen glaucoma patients was 40–80 years old. Patients who do not have a glaucoma diagnosis were chosen to represent the normal class. The four experts annotated each of these photographs. Three of the four ophthalmologists' opinions were sought before the standard was issued.

There are currently 15 pictures of healthy patients, 15 pictures of patients with diabetic retinopathy, and 15 pictures of patients with glaucoma in the public database HRF. Each subgroup includes one image of a healthy fundus, one of a patient with diabetic retinopathy, and one image showing glaucoma. The sizes of the images are 3,304 x 2,336 with a 22/23 split between training and testing images. For every image, binary gold standard vessel segmentation images are supplied. Additionally, for specific datasets, the masks determining the field of view (FOV) are provided. A team of specialists in the field of retinal image analysis and physicians from the affiliated ophthalmology clinics create the gold standard data. In order to assist with the evaluation of algorithms that localize the macula, optic disc, or distinguish between arteries and veins, researchers plan to add more gold standard data to the current images. A cooperative research team created this database to facilitate comparative analyses of automatic segmentation techniques on retinal fundus pictures. Research can be conducted using the database at no cost. Under a Creative Commons 4.0 Attribution License, researchers make it available.

650 photographs from the Singapore Malay Eye Study (SiMES) are part of the Online Retinal Fundus Image Dataset for Glaucoma Analysis and Research (ORIGA) database. The Singapore Eye Research Institute (SERI) is the organization behind SiMES. Experts annotated the photographs. The purpose of this dataset is to supply benchmark segmentation and classification algorithms with clinical ground truth. It generates manual segmentation for the optic disk and optic cup using a specially designed tool. In addition, it classifies each image as either healthy or glaucomatous and offers the cup-to-disk ratio. This dataset has been a standard in some of the most recent cutting-edge studies for the categorization of glaucoma.

The private dataset composed of retinal fundus images of 631 infected cases and 1080 normal cases. These images have been collected from various private hospitals, after consulting the ophthalmologists working there, located in the township of authors.

The given below Eqs. 1-17 is a short mathematical representation of the features that were retrieved

1. **CDR (Cup Disc Ratio) –**The eye is considered normal. The formula to calculate CDR is:

$$Cup\_\text{Disc\_Ratio} = \frac{Dia\_\text{of}\_Cup}{Dia\_\text{of}\_\text{Disc}} \tag{1}$$

2. **GLCM (Grey Level Co-occurrence Matrix) –**Grey level Co-occurrence Matrix $S(o, t)$:

$$S_m(o) = \sum_{t=1}^{P_k} S(o,t) \tag{2}$$

$$S_n(o) = \sum_{t=1}^{P_k} S(o,t) \tag{3}$$

$$S_{m+n}(k) = \sum_{o=1}^{P_k} \sum_{t=1}^{P_k} S(o,t) \tag{4}$$

$$A_{mn1} = -\sum_{o} \sum_{t} S(o,t) log\left\{S_m(o)S_n(t)\right\} \tag{5}$$

$$A_{mn2} = -\sum_{o} \sum_{t} S(o,t) log\{S_m(o)S_n(t) log\left\{S_m(o)S_n(t)\right\} \tag{6}$$

3. **SRE (Short Run Emphasis)–**

$$SRE = \frac{\sum_{l=1}^{s_g} \sum_{m=1}^{p_r} \frac{p(l,m,\theta)}{m^2}}{p_r(\theta)} \tag{7}$$

Here $p(l,m)$, $(l,m)^{th}$ element define the number of run with grey level l and length m in the image.

$$\textbf{LRE(Long Run Emphasis)} - LRE = \frac{\sum_{l=1}^{s_g} \sum_{m=1}^{p_r} p(l,m,\theta).m^2}{p_r(\theta)} \tag{8}$$

4. **GLU (Grey Level Uniformity)–**

$$g(i,j) = 255 - \frac{g(i,j) - g_{\min}}{g_{\max} - g_{\min}} \tag{9}$$

where $g_{\max}$ and $g_{\min}$ correspond to the maximum and minimum gray levels respectively and the whole range of gray levels is 255-0.

5. DDLS (Disc Damage Likelihood Scale)-

$$\text{Disc\_}Dam\text{\_Like\_Scale} = \frac{Rim\text{\_of\_Width}}{\text{Diameter\_of\_Disc}} \tag{10}$$

6. **Bicoherence-**

$$c(w_1,w_2)=\frac{E_M\left[M(w_1)M(w_2)M^*(w_1+w_2)\right]}{\sqrt{E_M\left[\left|M(w_1)M(w_2)\right|^2\right]M_X\left[\left|X(w_1+w_2)\right|^2\right]}}=\left|X(w_1,w_2)\right|e^{j\phi(X(w_1,w_2))} \tag{11}$$

$\left|X(w_1,w_2)\right|$ is a magnitude feature and $e^{j\phi(X(w_1,w_2))}$ is a phase feature.

7. **Energy-**

$$\text{energy}=\sum_{i=1}^{N_k}\sum_{j=1}^{N_k}p(i,j)^2 \tag{12}$$

8. Homogenity –

$$homop=\sum_{i=1}^{N_k}\sum_{j=1}^{N_k}\frac{p(i,j)}{1+|i-j|^2} \tag{13}$$

9. **Correlation-**

$$\text{correlation}=\sum_{i=0}^{M-1}\sum_{j=0}^{M-1}\frac{\{i\times j\}\times p(i,j)-\{\mu_x\times\mu_y\}}{\sigma_x\times\sigma_y} \tag{14}$$

10. Contrast-

$$contr=\sum_{i=1}^{N_g}\sum_{j=1}^{N_g}(i,j)^2p(i,j) \tag{15}$$

11. Dissimilarity (dissi)-

$$dissi=\sum_{i=1}^{N_g}\sum_{j=1}^{N_g}|i-j|p(i,j) \tag{16}$$

12. Entropy-

$$ENTROPY=-\sum_{i=0}^{G-1}\sum_{j=0}^{G-1}P(i,j)\times\log(P(i,j)) \tag{17}$$

A comprehensive collection of 36 features has been derived from the images provided. The list of features can be located in Table 3. Figure 2 explicates the diagrammatic view of proposed prediction system for detection and classification of glaucoma.

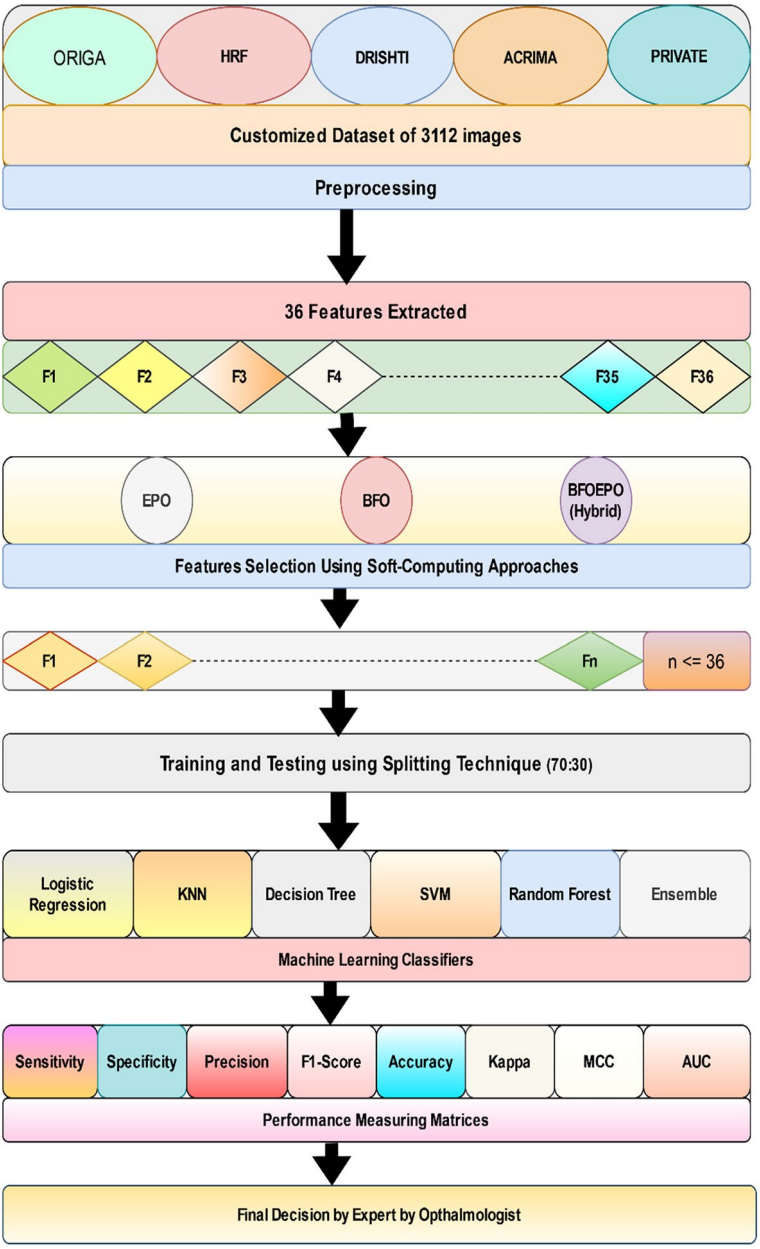

Fig 2 Diagrammatic view of the proposed work for glaucoma recognition

3.2 Feature selection algorithms

This research study has selected three nature inspired algorithms, namely EPO, BFO, and their hybrid variant, for inclusion (Fig. 3). Kindly locate the precise particulars of

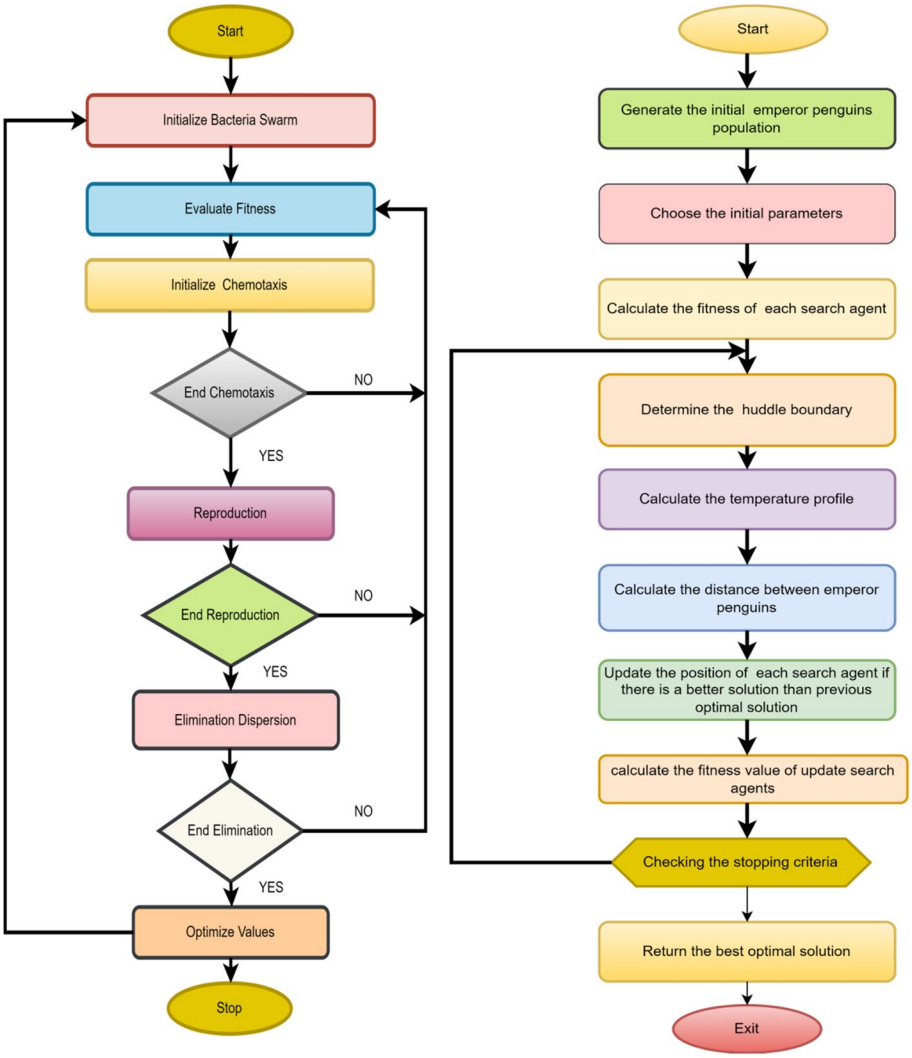

Fig. 3 Flowchart of BFO and EPO algorithm

the algorithms presented hereafter. The parameters and related values that were assigned throughout the execution of the three algorithms are shown in Table 3.

Table 4 displays the parameters and the associated values used in the algorithms. Equation (18) describes the objective function (Rastrigin Function) for each optimization process.

$$f(x) = \sum_{i=1}^{n} \left[xi^2 - 10\ cos(2\pi xi) + 10\right] \tag{18}$$

The hybrid BFOAEPO algorithm's pseudocode is shown below:
Step 01: Load the dataset for experimentation
Step 02: Initialize the BFOA parameters.
Step 03 : Produce a Sample Size for further study X(i=1,2,…,PopSize)(by BFOA)
Step 04: For t=1 to Max_iters
Step 05: The loops of elimination and dispersion
Step 06: Loop of reproduction
Step 07: Perform the computation on the fitness function.
Step 08: Eliminate unpromising bacteria(s).
Step 09: Update population (by EPO)
Step 10: Set the initial EPO parameters.
Step 11: Perform the computation on the fitness function.
Step 12: if (better solution is obtained) then update the current best
End if.
Update y=y+1
End For
Step 13: Return the optimal solution.

Three algorithms BFO, EPO and their hybrid are shortlisted for this study, whose details are given below. The Table 4, shown above, depicts the various parameters and their values assigned during the implementation of these three algorithms.

Novel nature-inspired optimization algorithms include the Bacteria Foraging Optimization Algorithm (BFO) [70, 71]. Tensile flagella propel the real bacteria during foraging. Flagella help E.coli forage by falling or swimming. Each flagellum pulls on the cell while spinning clockwise. Thus, the flagella move independently and the bacteria tumbles less, but in a dangerous environment, it tumbles often to find a nutritional gradient. Bacteria move swiftly by rotating flagella counterclockwise. Bacteria use chemotaxis to migrate toward a food gradient and avoid unpleasant conditions in the algorithm above. In friendly environments, pathogens spread. When they have enough food, they expand and break in the middle to make an identical clone at the right temperature. Passino added a replication event to BFO algorithm because to this. Chemotactic development may be disturbed by environmental changes or an attack, and a group of bacteria may travel or join the swarm. An elimination-dispersal event in a real bacterial community kills all germs or disperses a subpopulation into a different location [70, 71]. BFO algorithms parameters are displayed in Table 5.

The mathematical equations used in the algorithms are as follows

$$\mu(j) = \frac{\Delta(j)}{\sqrt{\Delta(j)^M \Delta(j)}} \tag{19}$$

$$\aleph^j((k+1,l,m) = \aleph^j(k,l,m) + A(j)\mu(j) \tag{20}$$

$$\begin{aligned} Bcc\left(\aleph, \aleph^i(k,l,m)\right) &= \sum_{j=1}^{o}\left[-r_{\text{attract}} exp1\left(x_{\text{attract}} \sum_s^h \left(\aleph_d - \aleph_d^j\right)^2\right)\right] \\ &+ \sum_{j=1}^{o}\left[-h1_{\text{repellant}} exp1\left(x_{\text{repellant}} \sum_s^h \left(\aleph_d - \aleph_d^j\right)^2\right)\right] \end{aligned} \tag{21}$$

$$F(j,k,l) = F(j,k,m,l) + Bcc\left(\aleph, \aleph^{j}(k,l,m)\right) \tag{22}$$

$$Q_r = \frac{Q}{2} \tag{23}$$

The emperor penguin is one of the largest, with male and female being similar in size. Emperor penguins have black backs, white bellies, golden ear patches, and grayish-yellow breasts. The emperor penguin's wings are a fin when swimming. Emperor penguins walk like people. The Antarctic winter can reach - 60 °C, but they live their entire lives there and are known for reproducing. Their distinctive feathers and body fat shield them from cold winds, but in extreme cold, they must congregate. During mating season, each female penguin lays one egg, which a male take. After egg transfer, females will seek up to 80 kilometers at sea. The eggs survive because male penguins keep them warm in their brood pouches. When a female emperor penguin returns to the nest after two months in the ocean, she vomits food for the babies to eat and care for. Emperor penguins are great swimmers and divers. The pair often hunt and forage. Only these creatures survive Antarctic winter by huddling. A mathematical model was created by dividing emperor penguin huddling into four stages. Emperor penguins randomly construct huddle boundaries. Second, they calculate their surroundings' temperature. Third, the method simplifies emperor penguin exploration and exploitation by computing penguin distances. Th approach decide the effective mover is best and recalculate the huddle's boundaries by rearranging the emperor penguins. Discovering the best mover is the goal of this mathematical approach. Huddles are on 2D polygonal L-shaped surfaces. The EPO algorithm was devised to combat this huddling [72].

The steps of EPO algorithms are as follows

Step 01: Generate the Emperor Penguins Population
Step 02: Set Initial Parameters such as Maximum Iterations, Temprature, A,C
Step 03: Calculate the fitness values for all search agent
Step 04:Determine the Huddle Boundary for Emperor Penguins Using:

$$\Re = \nabla\beta \tag{24}$$

$$\omega = \beta + i\xi \tag{25}$$

Step 05: Calculate temperature profile ($Temp'$) around the Huddle using:

$$Temp' \leftarrow \left(Temp - \frac{\mathbb{Z}_{iter}}{\psi - \mathbb{Z}_{iter}} \right) \tag{26}$$

$$Temp = \begin{cases} 0 & , \quad if \quad R* > 1 \\ 1 & , \quad if \quad R* < 1 \end{cases} \tag{27}$$

Step 06: Compute the distance between the emperor penguins using:

$$\overrightarrow{Dis_{ep}} = Abs\left(S1(\vec{A}).P1(\vec{x1}) - \vec{c1}.\overrightarrow{P1_{ep}(x1)} \right) \tag{28}$$

Step 07: Update the position of Emperor Penguins

$$\overrightarrow{P1_{ep}}(x1+1) = \overrightarrow{P1(x)} - \vec{\partial}.\overrightarrow{Dis_{ep}} \tag{29}$$

Step 08: If any emperor penguin goes beyond the Huddle Boundary improve its position.
Step 09: Calculate the fitness values for each search agent and update new optimal solution position
Step 10: If Stopping Criteria met STOP else Goto Step 28
Step 11: Return Best Emperor Penguins/Optimal Solutions

The mathematical equations applied in the algorithm are as follows Let γ defines the wind velocity and $\mathfrak{F}$ be the gradient of γ.

$$\mathfrak{F} = \Delta\gamma \tag{24}$$

Vector $\mathfrak{R}$ is combined with γ to generate the complex potential al

$$AF = \gamma + j\mathfrak{R} \tag{25}$$

where j denotes the imaginary constant and AF is an analytical function on the polygon plane.

The temperature profile around the huddle A' is computed as follows:

$$A' = \left(A - \frac{\text{Maximum}_{\text{iteration}}}{y - \text{Maximum}_{\text{iteration}}}\right) \tag{26}$$

$$A = \begin{cases} 0, & \text{if} \quad \text{Radius} > 1 \\ 1, & \text{if} \quad \text{Radius} < 1 \end{cases} \tag{27}$$

Here y define the current iteration, $\text{Maximum}_{\text{iteration}}$ represents the maximum number of iteration. A is the time for finding best optimal solution in a search space.

$$\overrightarrow{Dis_{epn}} = Abs\left(k\left(\overrightarrow{A1}\right).\overrightarrow{l(y)} - \overrightarrow{c1}.\overrightarrow{l_{epn}(y)}\right) \tag{28}$$

where $\overrightarrow{Dis_{epn}}$ shows the distance between the emperor penguin and best fittest search agent. y shows the current iteration. $\overrightarrow{A1}$ and $\overrightarrow{c1}$ are used to avoid the collision between neighbors. $k()$ defines the social forces of emperor penguins.

$$\overrightarrow{A1} = \left(Mov \times \left(A' + \text{Poly\_grid}(Acc)\right) \times \text{Random}()\right) - A' \tag{29}$$

$$\text{Poly\_grid}(Acc) = Abs\left(\vec{l} - \overrightarrow{l_{epn}}\right) \tag{30}$$

Poly_grid(Acc) defines the polygon grid accuracy by comparing difference between emperor penguins and random function Random().

$$\overrightarrow{c1} = \text{Random}() \tag{31}$$

$$k\left(\overrightarrow{A1}\right) = \left(\sqrt{f.e^{-x/l}} - e^{-x}\right)^2 \tag{32}$$

where e defines the expression function. f and l are control parameters for better exploration.

The hybridization of Bacterial Foraging Optimization (BFO) and Emperor Penguin Optimization (EPO) for feature selection in medical image processing is as follows.

1. **Initialization:**
   - Initialize populations for both BFO and EPO with random solutions. These solutions represent different subsets of features.
2. **Bacterial Foraging Optimization (BFO) Phase:**
   - Evaluate the fitness of each bacterium in the BFO population using a fitness function based on the selected features.
   - For each bacterium, perform reproduction steps:
     - Select a random bacterium from the population.
     - If the fitness of the selected bacterium is better than the current one, update the current bacterium's position to move towards the better solution.
3. **Emperor Penguin Optimization (EPO) Phase:**
   - Evaluate the fitness of each couple in the EPO population. Couples represent different subsets of features.
   - For each couple, perform a mating process involving swapping features.
     - Evaluate the fitness of the new couple after the swaps.
     - If the fitness of the new couple is better than the original, update the couple in the population.
4. **Discharge Mechanism (EPO):**
   - Evaluate the fitness of each penguin in the EPO population.
   - Sort the EPO population based on fitness.
   - For penguins in the worst-performing part of the population, apply a discharge mechanism to update their features. This mechanism might involve random changes or other strategies to explore new solutions.
5. **Combining Solutions:**
   - After completing both BFO and EPO phases, compare the best solutions obtained from each algorithm.
   - Select the solution with the better fitness as the final solution.
6. **Iteration:**
   - Repeat the entire process for a predefined number of iterations or until convergence criteria are met.
7. **Output:**
   - The final output is the selected subset of features that optimizes the performance of the algorithm based on the given fitness function.

The hybridization of BFO and EPO combines the exploration capabilities of BFO with the mating and swap mechanisms of EPO.

3.2.1 Time complexity of EPO

1. Population initialization process requires O(n × d) time where n indicates the population size and d indicates the dimension of a given problem.
2. The fitness of each agent requires O(Maxiteration × n × d) time where Maxiteration is the maximum number of iteration to simulate the proposed algorithm.
3. The function S () requires O(N) time where N defines the social forces of emperor penguins for better exploration and exploitation.
4. Steps 2 and 3 is repeated until the termination criteria is satisfied which needs O(k) time. Hence, the total complexity of Steps 2 and 3 is O(n × Maxiteration × d × N). Therefore, the overall time complexity of EPO algorithm is O(k × n × Maxiteration × d × N).

3.2.2 BFO time complexity

The time complexity of BFO algorithm can be presented O(P × (Q × (R × T × (L + W) + D) + N)). In the given expression P means iteration number for elimination dispersal. Q shows reproduction iteration time,R describe the number of chemotaxis activity, T is the bacterial number, L is the calculation time for fitness function, W represent the time complexity for chemotaxis operations based on evaluation method, D represents the computation time for reproduction process and N shows the computation time for elimination dispersal module.

3.2.3 Hybrid BFOAEPO algorithm time complexity

The overall computational complexity of Hybrid of bacterial foraging optimization algorithm and emperor penguins optimization is O(Max Iteration × N^4 + (l × p × t × f)). The complexity depends on maximum iteration, elimination and dispersion, reproduction, fitness function computation and elimination bacteria for the BFO, additionally including the updating of EPO computational complexity.

4 Results and discussion

The primary objective of utilizing nature-inspired computing techniques is to reduce the initial set of extracted features so as to precisely classify subject fundus retinal images into two distinct classes. The aforementioned reduced features will subsequently be employed as input for various ML classifiers. A comprehensive process of twelve distinct tests has been conducted, employing all three algorithms. All experiments possess a common objective function. Within the confines of a particular experimental setting, the population size exhibits a range spanning from 5 to 20, with incremental intervals of 5. This population's performance is evaluated after a number of iterations, from 100 to 500, in increments of 100. The attributes (features) of the case with the lowest objective function value are chosen, and then this case's attributes are sent to the classifier. The remaining four instances are excluded from further analysis. The computed findings have been aggregated and are displayed in Tables 6, 7, 8, 9, 10, 11, 12, 13, 14, 15, 16, 17 and 18. The findings generated by the EPO algorithm are presented in Tables 6 and 7. Tables 10 and 11 have been allocated for the purpose of displaying the outcomes produced by the BFO algorithm, while Tables 14 and 15 have been specifically designated for showcasing the outputs obtained by the hybrid algorithm. The tables (Table 6, 10, and 14) display and record the occurrences in which the minimum fitness value is observed within the five sub-experiments. The data for Table 7 is collected from Table 6, where the minimal objective value and the solution with the highest value created for each performance evaluation indicator are shown (by applying different ML classifiers). So, as the solution(s), we have prepared two tables from all the tests conducted under the canopy of one nature inspired-computing algorithm (for example, Tables 8 and 9 are comprised of all the experiments conducted under the EPO algorithm). Table 9 (as well as Tables 13 and 17) indicates the maximum value generated for each performance metric. Thus, Tables 9, 13 and 17 demonstrate the maximum values generated for various metrics by the EPO algorithm, BFO method, and hybrid algorithm, respectively. Table 8 (as well as Tables 12 and 16) illustrates the best values provided for various performance measures when the number of features picked has the smallest count

(in the case of EPO). Consequently, Tables 8, 12, and 16 illustrate the best values generated for various performance measures when the number of selected features had the lowest count (in the case of the EPO, BFO, and hybrid algorithms, respectively). The computed results are graphically represented in Figs. 4, 5 and 6. The respective confusion metrics are depicted in Figs. 4, 5 and 6 respectively.

One of the most common applications of the DeLong test is to compare the area under the receiver operating characteristic curves (AUC) of two different models. The p-value that is obtained from the DeLong test is something that is used in order to determine whether or not the difference in AUC between the two models is statistically significant. In the experiment, p-value statistical testing was also performed. In the context of machine learning, accurately calculating the standard deviation can be a helpful way to assess the variability or consistency of model performance over several runs or datasets. Achieving accuracy in the standard deviation is one way to do this. Along with the computation of various ML performance metrics, standard deviation and p-value(two-tailed test) have also been performed.

4.1 Experiment results generated through the EPO algorithm

The best confusion matrices produced by the four tests through EPO algorithm are shown in Fig. 4

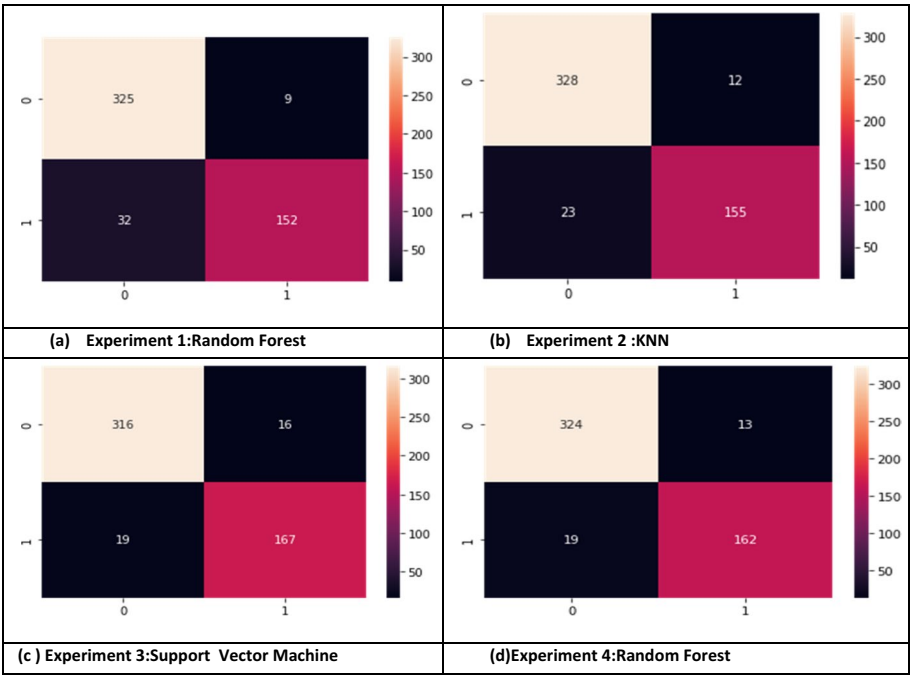

Fig. 4 Confusion Matrix of accuracy obtained by best classifier on split methodology **(a)** Least cost **0.82390** and PS 5 5 **(b)** Least cost **0.87603** and PS 10 **(c)** Least cost **0.78808** and PS 15 **(d)** Least cost **0.80926** and PS 20

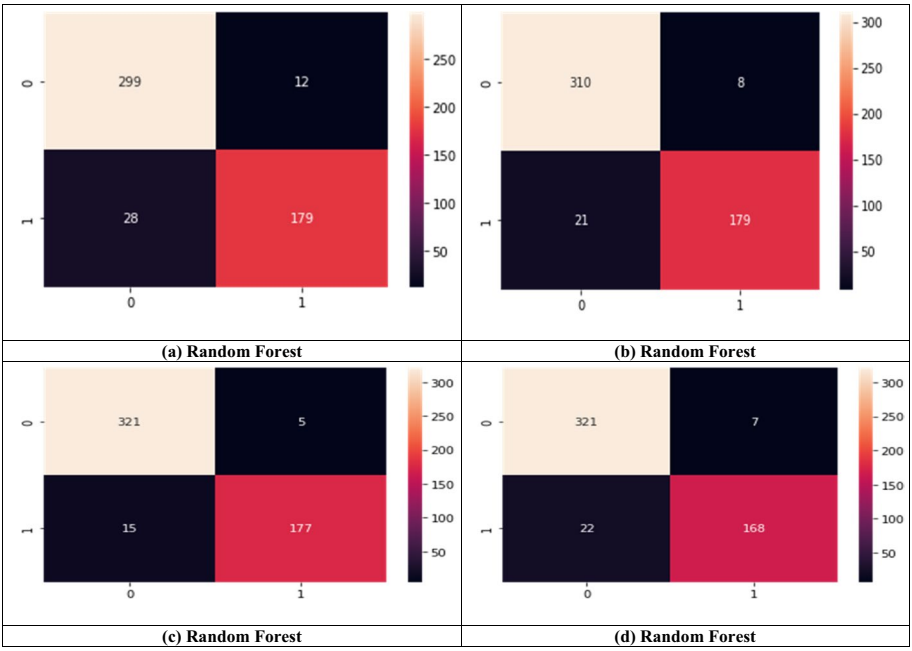

(a) Random Forest (b) Random Forest

(c) Random Forest (d) Random Forest

Fig. 5 Confusion Matrix of accuracy obtained by best classifier on splitting approach, **(a)** With least cost of **0.81045** (PS 5), **(b)** With least cost of **0.85425** (PS10), **(c)** With least cost of **0.82395** (PS 15), **(d)** With least cost of **0.75206** (PS 20)

4.2 Results computed after applying the splitting approach to the BFO algorithm in different experiments

The best confusion matrices produced by the four tests through BFO algorithm are shown in Fig. 5.

4.3 Experimental results computed with features returned by the hybrid algorithm

Tables 12, 13, 14, and 15 depicts the results generated through the proposed and implemented hybrid approach with population size 5 to 20 with variation of 5.

The best confusion matrices produced by the four tests through hybrid approach are shown in Fig. 6.

The Table 18 presents the final best results from three different perspectives. The first perspective showcases the best results achieved for a customized dataset. The next perspective displays the best generated results using our proposed approach for a private dataset. Lastly, the results generated through our approach for a public dataset are shown in the last perspective.

4.4 Discussion and analysis

The proposed solution encompasses the utilization of three distinct algorithms: BFO, EPO, and a hybrid approach that amalgamates the functionalities of both algorithms. The

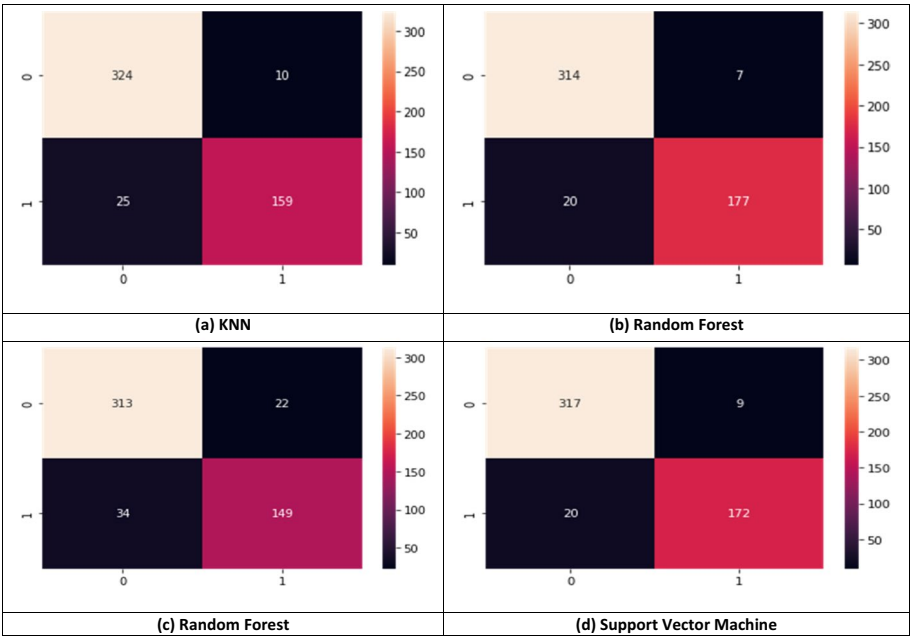

Fig. 6 Confusion Matrix of accuracy obtained by best classifier on splitting approach, **(a)** With least cost of **0.81865** (PS 5)**, (b)** With least cost of **0.88075** (PS 10), **(c)** With least cost of **0.76834** (PS 15), **(d)** With least cost of **0.83461** (PS 20)

objective of these algorithms is to minimize the initial feature set that will be inputted into various ML classifiers, with the aim of classifying the subject fundus images into two distinct categories. A comprehensive investigation of twelve distinct tests has been administered, utilizing all three methodologies. All experiments possess a common objective function. Within the confines of a particular experimental setting, the population size exhibits a range spanning from 5 to 20, with increments occurring at intervals of 5. Through a methodical modification of the number of iterations, ranging from 100 to 500, with increments of 100, the performance of the population is evaluated. The properties, which are also known as features, of the instance that exhibits the lowest value of the objective function are then sent to the classifier. The study does not include and does not take into account the other four occurrences. The information in the aforementioned tables indicates that a minimum of 4 features may be collected and a maximum of 28 features. As a result, the level of feature reduction might be as high as 88.88% (4 out of 36) or as low as 22.22%. The timing of an execution must be determined by taking into account two different viewpoints. The main focus is on demonstrating the length of iteration for nature inspired computing methods, followed by an examination of the time needed for developing and testing machine learning models. The first six ML classifiers have qualities that are commonly associated with classical techniques, while the seventh one composition combines aspects from the first six. A variety of measures, including accuracy, sensitivity, specificity, and precision, as well as the F1-Score, Kappa-Score, Matthews Correlation Coefficient (MCC), and Area Under the Curve (AUC), are used to assess classifier performance. Each of these metrics plays a pivotal role in the prognosis of human diseases based on medical images. The simultaneous observation of all these computations within a single research study is infrequent.

The accuracy of our model refers to the ratio of correct predictions to the total number of predictions made [10]. The determination of the accuracy rate involves the division of the count of accurate forecasts by the overall count of predictions. The metric of accuracy holds significant importance as a performance indicator, and our findings in this regard are noteworthy. By combining the hybrid algorithm with the Random Forest classifier, a remarkable accuracy rate of 96.55% was attained. The hybrid case exhibits the lowest accuracy rate of 89.180%, followed by the BFO case with an accuracy of 85.902%, and the EPO case with an accuracy of 87.065%. The proposed method demonstrates a notable degree of precision. The concept of sensitivity holds significant importance in the context of measurement, specifically in relation to the test's capacity to effectively identify individuals who genuinely suffer from the disease. The sensitivity of a medical test, also referred to as the "detection rate" in clinical contexts, pertains to the ratio of individuals who yield positive test results for a particular illness among those who genuinely possess the ailment. A diagnostic test with a sensitivity of 100% will accurately identify and categorize every individual with the specific condition as positive. According to the EPO analysis, the sensitivity results reveal that RF exhibits the highest score of 0.8974. In a similar vein, the sensitivity score for BFO is recorded as 0.92187. In regard to the hybrid models, the utilization of a decision tree methodology results in the attainment of the highest sensitivity score, specifically 0.934780.

The notion of specificity pertains to the capacity of a diagnostic test to effectively discern individuals who do not manifest any symptoms and are in a state of optimal health. The concept of "specificity" refers to the proportion of individuals who do not have a particular disease and obtain a negative result when tested [14]. A positive outcome suggests a high probability of the presence of the condition. A test with perfect specificity would correctly identify all individuals who do not have the condition by producing a negative result, while a test with imperfect specificity would conclusively demonstrate the absence of the sickness. As the efficacy of this strategy can be seen in the range of values acquired, the criteria of creating specificity is of the biggest significance and must be properly taken into consideration. The range of EPO, when taking into account the random forest (RF), spans from 0.9029 to 0.99401. The range of BFO values spans from 0.88745 to 0.98466. The hybrid method, taking into account RF, exhibits a range of values spanning from 0.91616 to 0.99376. As a result, a specificity rate of 90% was achieved in all scenarios, with the random forest algorithm demonstrating superior efficiency as a classifier. The F1-score is determined by taking the harmonic mean of accuracy and recall, resulting in a well-balanced evaluation metric for the classifier. The F1-score is a performance measure commonly employed in the evaluation of classification models. It is designed to assess accuracy by considering the impact of both false positives and false negatives. The combination of EPO-RF yields a maximum F1-score value of 0.91001, while the BFO combination achieves a maximum F1-score value of 0.9215. Additionally, the hybrid-RF configuration achieves a maximum F1-score value of 0.9386. Precision is the ratio of correctly identified positive cases to all the cases that are identified as positive [73]. It is feasible to accurately ascertain the prevalence of glaucoma among individuals. Moreover, the degree of precision has a direct influence on the quantity of significant data points. It is crucial that we exercise caution in commencing treatment for a patient who, according to our theoretical framework, displays symptoms suggestive of glaucoma but does not manifest the actual pathological state. The precision values for EPO, BFO, and the hybrid approach are 0.98387, 0.9722, and 0.98876, respectively, at their maximum values.

Each diagnostic threshold is accompanied by a corresponding set of sensitivity and specificity values. In order to construct a Receiver Operating Characteristic (ROC) curve,

the dataset was utilized to plot pairs of data points, with the x-axis representing specificity and the y-axis representing sensitivity [74]. Both the computation of the AUC and the examination of the characteristics of the ROC curve can be utilized to evaluate the discriminative capacity of a specific test. As the curve gradually approaches the upper left corner and the area beneath it expands, the test demonstrates enhanced discriminatory capacity in discerning between afflicted and non-afflicted states. The integral of the curve, which is a dependable indicator of the effectiveness of the test, can assume values within the range of 0 to 1. The non-selective region of a test is characterized by an area of 0.50, whereas an ideal diagnostic test exhibits AUC of 1. The AUC is a widely accepted measure utilized for assessing the diagnostic precision of a given test. Furthermore, we have computed the AUC scores, which exhibit favourable outcomes in this specific context. The combination of the EPO algorithm and the RF classifier yielded AUC scores ranging from 0.8764 to 0.9698. In a similar vein, the BFO algorithm demonstrated AUC scores spanning from 0.9010 to 0.9763, whereas the hybrid algorithm, incorporating the RF classifier, exhibited AUC scores ranging from 0.9078 to 0.9799. As the value approaches 1.000, the quality of the output increases. The hybrid technique stands out among the classifiers due to its extensive performance range, reaching a maximum value of 0.9799. However, the Random Forest classifier demonstrates superior performance in relation to the AUC metric. The results encompass a range of important parameters, such as ROC curves for each instance, confusion metrics, and calculations of MCC and Kappa scores for each experiment.

5 Comparison with the current best practices

Table 19 provides an evaluation of the proposed technique compared to the current state-of-the-art glaucoma prediction approaches. This comparison table demonstrates the efficacy of the applied method in identifying glaucoma relative to earlier research. This table shows strong evidence that the suggested method is reliable and good at classifying fundus pictures. Compared to earlier research, the used method is up to 96.55% accurate at finding glaucoma. As with other measures, the performance's sensitivity and specificity are also both auspicious. When compared to the other 20 methods indicated in Table 19 that were published in or after 2018, our performance displays excellent results. In a few instances, our approach, which leverages nature inspired computing and ML techniques, has exhibited superior efficacy when compared to deep learning (DL) methodologies. In a few situations, however, the datasets against which the other techniques were tested may vary. In our case, multiple datasets have been analyzed to determine the generalizability of our proposed method, as we have worked on them to assess the performance of the previously disclosed strategy.

In this discussion about how our study compares to other research, our results have been compared to those of the fifteen studies listed in Table 16. This has allowed for a thorough look at the topic. The use of DL algorithms for the evaluation of the characteristics of the OC and OD has received significant attention recently in the field of glaucoma research. A plethora of studies have been published in this field. According to researchers, delays in treatment can be attributed to the time-consuming manual input required from ophthalmologists in conventional methodologies, specifically the need for measurements of disc and cup sizes during screening. Hence, it is crucial to enhance the progress of more effective and accurate diagnostic instruments for the detection of glaucoma. The practical and efficient identification of glaucoma can be achieved through the utilization of automated

techniques. The evaluation of the OD and OC plays a crucial role in the diagnosis of glaucoma. The primary aim of the proposed methodologies is to achieve precise segmentation of the OD and OC from a fundus image. The dataset utilized in the study comprised 101 Drishti GS1 images and 650 ORIGA images [75]. The process of segmenting OD and OC, along with calculating the CDR and evaluating the four sections of the neuro-retinal rim (NRR), was conducted. The researchers exhibited an accuracy rate of 76.42%, a sensitivity rate of 0.799, and a specificity rate of 0.738. In contrast to the findings of previous studies, our results exhibit a higher level of performance across all three metrics. The authors of [76] presented an effective approach for segmenting the OC and OD using semi-supervised conditional generative adversarial networks (GANs). The performance evaluation of the proposed method was carried out using two datasets: ORIGA, which comprises 650 fundus images consisting of 168 eyes with glaucoma and 482 eyes without glaucoma, and REFUGE, which consists of 400 fundus images including 40 eyes with glaucoma and 360 eyes without glaucoma. As the training set for their study, the researchers have chosen a dataset that consists of 300 fundus images with precise annotations. Out of the available options, a total of 30 images can be attributed to individuals diagnosed with glaucoma. The remaining images have been assigned to the testing set. The accuracy values for the ORIGA and REFUGE datasets were determined to be 76.57% and 82.78%, respectively. The sensitivity values for the ORIGA and REFUGE datasets were calculated to be 0.7273 and 0.7, respectively. Furthermore, the specificity values for the ORIGA and REFUGE datasets were determined to be 0.8041 and 0.7, respectively. The overall specificity was calculated to be 0.956. In the following study [77], the authors presented two sophisticated glaucoma detection techniques that employed deep learning methodologies. The M-Net is a multi-label segmentation network that combines the segmentation of an OD and an OC. The U-shaped convolutional network of M-Multi-scale Net was utilized to generate a segmentation probability map. This network incorporates a side-output layer to facilitate the learning of discriminative representations. The assessment of glaucoma risk was performed by employing the vertical CDR, which was obtained through the segmentation of the optic disc and cup. The second network employed in the study is known as the disc-aware ensemble network, abbreviated DENet. The network successfully integrates the local optical disc region with the deep hierarchical context of the global fundus image. The DENet algorithm provides a glaucoma detection result without requiring the use of image segmentation techniques. The researchers used the Singapore Chinese Eye Study dataset, which includes 1676 images and 46 cases of glaucoma, along with the ORIGA dataset. Additionally, a dataset derived from a population-based study was incorporated, encompassing 5783 eye images, with 113 eyes affected by glaucoma and 5670 eyes classified as normal. The obtained outcomes encompass an accuracy rate of 84.29%, a sensitivity rate of 0.8478%, and a specificity rate of 0.8380%. Upon comparing our findings with this particular strategy, we have observed that our outcomes have been significantly superior. The utilization of a lightweight, deep architecture for the detection of glaucoma has been documented in a study, demonstrating its ability to carry out segmentation and classification tasks [46]. The training and testing procedures involved the incorporation of a combined total of 2482 images from the ORIGA dataset and other datasets that were deemed relevant. After that, the above networks were used to make a glaucoma assessment system that gives a clear diagnosis of glaucoma, a range of morphological measurements, and segmentations of relevant anatomical parts. In relation to the classification metrics, the obtained outcomes encompass an accuracy rate of 87%, a sensitivity value of 0.85, and an AUC score of 0.93. Upon conducting a comparative analysis between our endeavors and the findings of this study, it becomes apparent that our results exhibit a similar level of excellence.

The system under consideration initially employed a DeepLabv3+ architecture for the purpose of segmenting the optic disc region. Nevertheless, the encoder module was later replaced with several deep CNNs [78]. The experts used three ways to put things into groups: (1) transfer learning, (2) learning the feature descriptors using SVMs, and (3) putting together groups of approaches that came from (1) and (2). The researchers' research study involved a thorough analysis of five different datasets, including REFUGE, ACRIMA, ORIGA, and additional datasets. These datasets collectively encompassed a total of 2787 retinal images. The study's findings indicate that a combination of DeepLabv3+ and MobileNet proves to be the most efficacious method for segmenting the OD. The integration of various methodologies demonstrated superior performance compared to current approaches in the classification of glaucoma. The achieved accuracy scores were 97.37%, 90.00%, 86.84%, and 99.53%, with corresponding AUC ratings of 100%, 92.06%, 91.67%, and 99.98%.The empirical study [79] employed DL-based techniques to achieve two primary objectives: the segmentation of the OD and OC and the classification of glaucoma. REFUGE provides the general public with unrestricted access to an extensive compilation of data that is currently unparalleled in its breadth and depth. The dataset consists of a thorough compilation of 1,200 fundus images, along with precise segmentations and clinical glaucoma labels. The researchers encountered limitations in their ability to provide data pertaining to precision and specificity. Nevertheless, a sensitivity value of 0.9752 was successfully determined. The absence of certain crucial elements, such as precision and specificity, in the discourse is noteworthy, particularly in light of the fact that our findings surpass the suggested ones. The authors proposed the utilization of an enhanced UNet++ neural network for the simultaneous segmentation of the OD and OC, with the region of interest (ROI) serving as the foundation, as suggested in a previous study [80]. The calculation of the cup-to-disc ratio was performed using the segmentation outcomes. When the increasing field of view (IFOV) feature was added, the goal was to get all the textural properties, statistical features, and other hidden image-based data. Subsequently, the most suitable feature combination is selected from a comprehensive set of all feasible feature combinations. In order to mitigate the problem of imbalanced training data, the adaptive synthetic sampling technique is subsequently employed. The development of the gradient-boosting decision tree (GBDT) classifier was specifically focused on its application in glaucoma screening. Experimental results using 650 images from the ORIGA dataset show that the algorithm suggested in this study exhibits glaucoma screening performance. The algorithm achieves a sensitivity of 0.894%, an accuracy of 0.843%, and an AUC of 0.901. Upon conducting a comparative analysis between our findings and the outcomes of the aforementioned study, it becomes evident that our results exhibit a superior level of quality. This study presents a novel methodology for classifying glaucoma, employing a solitary deep CNN [82]. A determination was made to choose a combined total of 10,658 photographs from the subsequent sources: Refuge 24, Origa 25, LAG 26, Drishti-GS127, sjchoi86-HRF 28, HRF 29, and ODIR 30. The attained accuracy of 95.3%, sensitivity of 0.841, and specificity of 0.958% fail to exceed the performance of our suggested approach. The fundus image underwent processing using a CNN consisting of 18 layers, which was constructed and trained. The objective of this procedure was to identify and extract the distinctive characteristics that are present within the image. The model's architecture comprises a fully connected layer, two max-pooling layers, and four convolutional layers. The use of a two-stage tuning technique is advised for the purpose of determining an appropriate batch size and initial learning rate. The network evaluation was performed utilizing several databases, namely DRISHTI-GS1, ORIGA, RIM-ONE2 (version 2), ACRIMA, and large-scale

attention-based glaucoma (LAG) databases. The DRISHTI-GS1, RIM-ONE2, ORIGA, LAG, and ACRIMA databases exhibited overall accuracy rates of 86.62%, 85.97%, 78.33%, 94.43%, and 96.64%, respectively. Through the utilization of the ACRIMA database, the approach put forth in this study demonstrated a sensitivity value of 0.5806 and a specificity value of 0.9244. The findings of our study exceed the previously documented results, encompassing both our own dataset and the ACRIMA dataset. A better deep learning-based custom UNET++ model [83] was created by the researchers to predict glaucoma. It does this by using a new segmentation technique to separate the OD and OC. The application of the Dhristi dataset led to improved presentation on a restricted dataset. The development of the segmentation-specific model involved the utilization of a modified loss function and the implementation of hyperparameter tuning techniques. The loss function that has been recently developed successfully addresses the problem of class imbalance caused by the limited dimensions of the optic nerve head. To classify a set of 650 ORIGA images as either glaucomatous or non-glaucomatous, the ISNT criteria's clinical feature was employed. The proposed methodology successfully distinguishes between images displaying indications of glaucoma and those that do not, achieving a 96% success rate by identifying pertinent clinical characteristics. The sensitivity and specificity values obtained were 0.87 and 0.81, respectively. After conducting a comparative analysis of our empirical investigation with other relevant studies, it becomes apparent that our findings outperform theirs across all three criteria. The methodology employed in this study entailed the implementation of an automated system utilizing the Deep CNN architecture known as Glaucoma Network (G-Net) [84]. The utilization of this system was implemented to discern between the OD and OC within retinal fundus images. The proposed methodology employs a dual neural network architecture with the objective of segmenting the optic disc and cup. The model achieved a segmentation accuracy of 95.8% for disc segmentation on a dataset consisting of 50 fundus images. Additionally, the model demonstrated an accuracy of 93% for cup segmentation. The methodology utilized in this research entails the concurrent operation of two neural networks, which yield segmentation accuracies of 95.8% and 93.2% for OD and OC, respectively. The accuracy, sensitivity, and specificity attained for the DRISHTI data set are 95.03%, 0.7379, and 0.8623, respectively. The obtained results exhibit a resemblance to our own research findings. This research paper introduces the application of the Grey Wolf Optimized Neural Network (GWO-NN) as a diagnostic tool for glaucoma. During the preprocessing phase, the input image is subjected to multiple steps. Initially, the image undergoes a conversion process to grayscale. Subsequently, the process of noise reduction is executed through the use of an adaptive median filter (AMF). Subsequently, the process of image normalization is implemented. The process of feature extraction was performed by utilizing GLCM features, which were derived from the image's energy, contrast, homogeneity, and correlation. Furthermore, the researchers employed SURF, HOG, and global features in their study. The extracted features comprised variance, mean, and standard deviation. The subsequent step involves the implementation of the classification procedure using the GWO-NN algorithm. The approach that was presented demonstrated an accuracy rate of 93.103%, a sensitivity rate of 0.916778, and a specificity rate of 0.94117. By comparing our proposed strategy to the suggested work, we can see how well our method works for both selecting features using a nature inspired computing approach and classifying them using machine learning classifiers. The results of our study clearly indicate a higher level of performance when considering all three comparable metrics. In addition, it is important to acknowledge that the authors of the aforementioned study [63] have not made the training and testing datasets accessible to the

public.This next study suggests that glaucoma can be found in fundus photographs by using image channels (ICs) and the DWT [85]. After the process of scaling the input images, the resulting outputs consist of the red channel (RC), green channel (GC), blue channel (BC), and grayscale (GS) images. Using the second-level (SL) discrete wavelet transform (DWT) makes it possible to improve and separate four different types of images into subband images (SBIs) that can be looked at separately. After that, the most important parts were taken out one by one from each of the sub-band images (SBIs) that were created using the DWT. Summation, normalization, and a numerical value assignment combine the extracted features from the RC, GC, BC, and GS images. The robust properties are incorporated into the least squares support vector machine (LS-SVM) classifier. The dataset employed for analysis was the RIM-1 dataset. A Zernike moment feature, seven Hu's invariant moment features, six Chip histogram features, thirteen basic texture features derived from GLCM, fourteen Haralick texture features, twenty-two advanced GLCM features, and seven grey level run length matrix (GLRLM) features were extracted from the dataset. These are based on the number of grey-level runs for different lengths. Combining the characteristics from the red channel (RC), green channel (GC), blue channel (BC), and grayscale (GS) images produced the composite image C-RGBGs-IF. The use of 10-fold cross validation resulted in the C-RGBGs-achieved IF exhibiting an accuracy of 84.95%, a sensitivity of 86%, and a specificity of 83.85%. After conducting a comprehensive comparison between our research findings and the existing empirical evidence, it is apparent that our findings demonstrate a higher level of potential. The authors [47] introduced a new methodology for the detection of glaucoma, employing FAWT to divide the pre-processed images into multiple sub-band images. The ReliefF and sequential box-counting (SBC) techniques were subsequently utilized to extract a variety of entropies and features derived from fractal dimension (FD). The aforementioned features encompass Kapur entropy (KE), Renyi entropy (RE), Yager entropy (YE), and the FD feature. In addition, Fisher's LDA was implemented to assess the obtained feature values. The categorization of glaucoma stages was performed by employing the LS-SVM classifier, which utilized the higher-rank features. The evaluation of the proposed method involved the utilization of a total of 941 images sourced from the glaucoma datasets RIM-ONE, ORIGA, DRISHTI, and HRF. The efficacy of the suggested methodology was assessed through the implementation of tenfold cross-validation. The findings demonstrate a classification accuracy of 93.4%, a sensitivity of 0.94, and a specificity of 0.8784. The findings presented exhibit a lower level of quality in comparison to our own results, as they were acquired through the utilization of a split-based approach with a ratio of 70:30. The study conducted by the authors focused on the retrieval of GIST, a method based on Gabor filters that extracts textural characteristics from fundus images, as well as pyramid histograms of oriented gradients (PHOG) features. These features were extracted from preprocessed fundus images. The authors employed these features in order to obtain a comprehensive shape description of fundus images [27]. The acquired attributes were assessed and selected by PCA to identify the most essential features. The classification of images into two categories, infected or normal, was performed using a SVM classifier. The assessment was carried out on a sample of sixty images, comprising both Drishti-GS1 and HRF images. The researchers' method yielded an accuracy of 83.4% and an AUC value of 0.88. Neither of these statistics meets the level of success that our planned technique enabled us to achieve. The calculation of sensitivity and specificity has not been performed.

If we examine the full description of the studies included in Table 19 that is provided above, we can observe that our study is distinct and superior in many aspects to the vast majority of the research addressed in Table 19. It is immediately apparent that the majority of the study has only examined OD, OC, and CDR. Other feature classes have gotten little consideration (or no importance). However, instead of focusing just on OD, OC, and CDR, our study focuses on a range of feature classes. The great majority of researchers have also employed DL-based methods (proposing the new model or customizing the available DL models). A few studies applying ML have also been published. The fact that feature extraction has not been commonly used in these studies is a fundamental component of our technique. Few studies have focused on feature selection (sometimes referred to as feature dimension reduction), and those that have used approaches like LDA and PCA have largely cited their results. Nevertheless, for this operation, we employed three nature computing techniques (for optimal feature selection), two recently proposed, and one hybrid of these from our side. We have also shown one of the three that is a hybrid of the other two, which sufficiently displays the uniqueness, novelty, and innovation of the presented work. We have employed a number of ML classifiers, including an ensemble of them; nonetheless, these classifiers are not commonly used in one work. In addition, we generated other statistical performance evaluation indicators, including execution time. Seldom does the analysis get published in such depth. Our method's results for performance evaluation metrics like accuracy, sensitivity, specificity, F1-score, and AUC are better (in almost all ways) than those of almost all previous research. This shows that our approach works in highly impressive fashion.

6 Advantages, limitations and future scope of the proposed work

The proposed approach demonstrates a high level of effectiveness in identifying the most influential features necessary for confirming the presence of the disease. This approach has the potential to be applied to any dataset in order to efficiently select features that are necessary for the classification of the problem being addressed. The suggested approach not only decreases the dimensionality of the search space but also reduces the training and testing time of the machine learning models. Simultaneously, this approach enhances the effectiveness of the classification models by eliminating unnecessary features. Owing to exemplary performance of the proposed approach indicate its potential to enhance the decision-making process for medical professionals by serving as a valuable second opinion. The presented system can also be implemented in areas with a limited number of skilled physicians.

Here are some of the limitations of this work. Relying solely on machines may not be suitable at this time, considering the importance placed on evidence-based medicine. Incorporating Macula scans, as well as publicly accessible features such as intraocular pressure (IOP) and visual test readings, would undoubtedly enhance the accuracy of the method. This task is limited to a single customized mid-size data set. It may be worth considering seeking external validation for the proposed method using larger and more varied data sets. There are potential benefits to be gained by increasing the sample size in the database. In order to facilitate real-time implementation, it may be beneficial to include

the out-of-sample data set. Utilizing sophisticated image processing and classification algorithms can enhance the accuracy of classification. Furthermore, properties that are not explicitly mentioned in the suggested approach may also be evaluated. Various hybrid variations of recent nature inspired computing-based techniques are suggested. It is possible that certain algorithms may exhibit superior performance in terms of accuracy, feature reduction, or a combination of both. We have assumed that the patient may have an eye infection, if any. The current focus is on classification, regardless of whether or not an individual has glaucoma. There is a lack of distinction in this work regarding the varying stages of glaucoma infection.

Other drawback of this study is its sole reliance on a single mid-size customized dataset for performance evaluation. However, by applying the recommended approach to additional datasets, the study's scope could be expanded even further. In addition, the exploration of different datasets could be considered for future studies. There is potential for expanding the range of features that can be extracted. In addition, the image was not preprocessed in our study to eliminate blood vessels. Our objective is to analyze the impact of this process on the ultimate classification outcome. Another important factor to consider is the classification phase. Given our focus on achieving efficient feature selection, we found that the evaluated classifiers needed further fine-tuning to reach their optimal performance. We are of the opinion that incorporating multi-objective methods into our approach would enhance our outcomes by enabling more accurate parameter tuning.

Glaucoma is a multifaceted systemic condition. Conducting a comprehensive analysis of the visual system could potentially enhance the accuracy of glaucoma diagnosis and prognosis. Through the utilization of cutting-edge neuro-imaging and retinal imaging technologies, the integration of data from different visual system components can lead to the accomplishment of this objective. For better results, future research in this field can explore various feature selection strategies and employ different classification approaches to enhance accuracy and efficiency. In order to enhance the system's overall accuracy and rectify misclassifications, it is recommended that future research explore the utilization of different features or the integration of texture, shape, and color features. A pressing issue revolves around evaluating the efficacy of specific features through the application of diverse statistical feature selection techniques. In addition, the development of a two-phase feature selection strategy presents an evaluation challenge and signifies a new avenue of research. The initial step of the strategy entails utilizing classical statistical methods for selection, while the subsequent step involves employing soft-computing approaches for selection. Evaluating the performance of different versions of the BFO and EPO, as suggested by researchers, poses yet another challenging problem. In addition, researchers are currently developing an advanced nature inspired-based optimization algorithm with innovative features. Thus, there is room for enhancing classification accuracy by integrating the recently introduced algorithms more effectively with highly efficient classifiers. The current issue can be reframed as a multi-objective problem, where the aim is to balance the selection of features and accuracy. Collaboration between ophthalmologists and machine-learning researchers remains essential for ongoing progress. By leveraging a strong blend of technical knowledge and deep industry experience, the potential for delivering highly efficient and impactful solutions is greatly enhanced. We will also explore the performance of the suggested approach on K-fold cross validation approach. For enhanced accuracy, there is potential to expand the scope of this work in the future by incorporating automation techniques, specifically by leveraging

deep learning methodologies and a more extensive dataset.. Future efforts can further enhance the current methodology by seamlessly integrating it with the graphical user interface designed for glaucoma diagnosis. Researchers are currently developing novel optimization algorithms inspired by nature. We will also investigate this avenue in order to identify a more efficient approach that surpasses the suggested method. The optimization problem at hand can be expressed using a multi-objective criterion. Additionally, a thorough review of the existing literature reveals that there has been limited research conducted in this particular area. Therefore, the exploration of feature selection using multi-objective criteria remains an untapped opportunity for future researchers. In the future, the deep cooperation between artificial intelligence and medical technology will make the datasets and clinical application rules more standardized, and glaucoma diagnosis and prediction tools will be simplified in a single direction, which will benefit multiple ethnic groups. In addition, it encompasses the skill to detect and identify various eye conditions, including diabetic retinopathy, macular edema, and retinal hemorrhage.

7 Conclusions

It is crucial to promptly identify glaucoma in order to effectively manage the advancement of visual impairment. Without appropriate medical intervention, this condition has the potential to advance and result in irreversible visual impairment. The challenging and time-intensive nature of traditional diagnostic procedures significantly impairs the efficacy of early detection and diagnosis of glaucoma. Moreover, a crucial task entails the identification and subsequent gathering of the most pertinent features(attributes). The main goal of this study is to introduce an innovative and effective feature selection strategy. The implemented strategy aims to identify the most influential features, resulting in a reduced feature space. Additionally, it is expected to enhance the overall performance of the classification system and reduce the training and testing time of machine learning models. To achieve the above-mentioned goals through the proposed strategy, this article provides an in-depth of the utilization of the EPO algorithm, the BFO algorithm, and a hybrid variant that combines both algorithms for the selection of most informative features. Based on our current understanding, there has been limited observation of the utilization of these algorithms for the detection of glaucoma. The features selected in these three algorithms are assessed using six machine learning classifiers. The presented approach is evaluated using benchmark fundus image datasets. Many tests have been conducted with the objective of identifying the optimal combination of selected features using a machine learning classifier. In the ideal situation, feature selection is able to achieve a remarkable rate, whereby only few features are preserved from the initial set of features, with no significant impact on accuracy. The performance has also been assessed using statistical measures, such as calculating the standard deviation of accuracy and conducting a p-value(two tailed test) test. The proposed methodology for the processing and analysis of high-resolution retinal images demonstrates both computational efficiency and a minimal time commitment. Ophthalmologists may consider employing the proposed methodology as an additional tool in the diagnostic evaluation of glaucoma. Hence, the proposed technique has the potential to provide significant advantages in the initial assessment of individuals diagnosed with glaucoma.

Appendix

Figure 7 depicts the look of the receiver operating characteristic (ROC) results produced by the EPO algorithm for all four algorithms. Figures 8 and 9 are devoted to the organization of the ROC produced by the BFO algorithm and hybrid algorithm, respectively for all four algorithms.

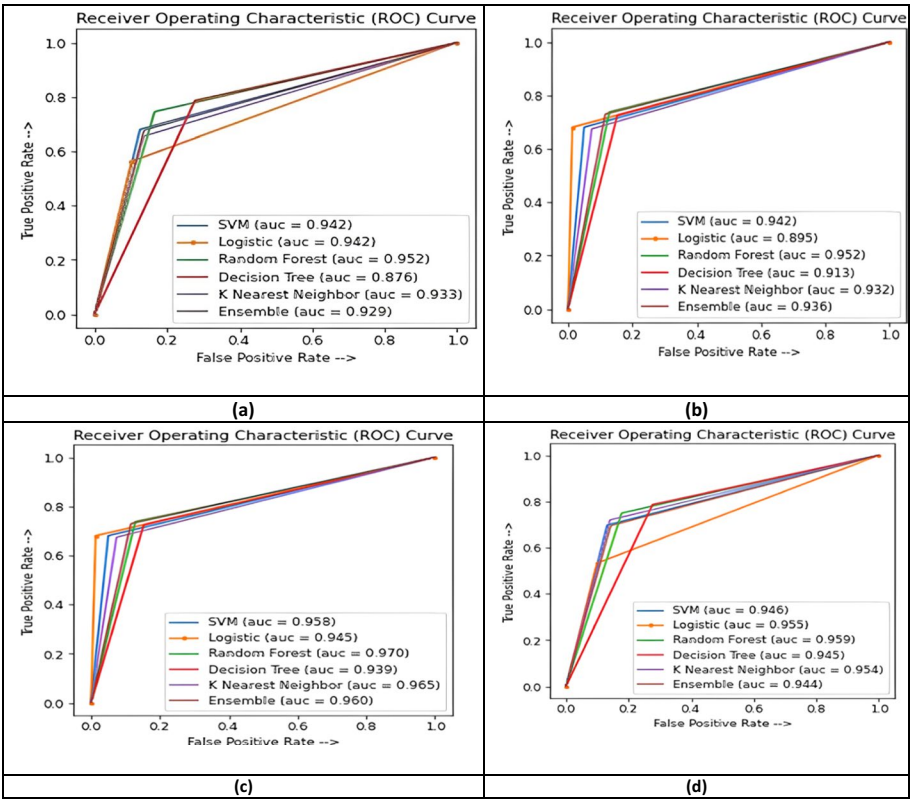

Fig. 7 Collective ROC curve of all ML classifiers with70:30 implemented approach, (**a**) Least cost **0.82390** and PS 5, (**b**) Least cost **0.87603** and PS10, (**c**) Least cost **0.78808** and PS 15 **(d)** Least cost **0.80926** and PS 20

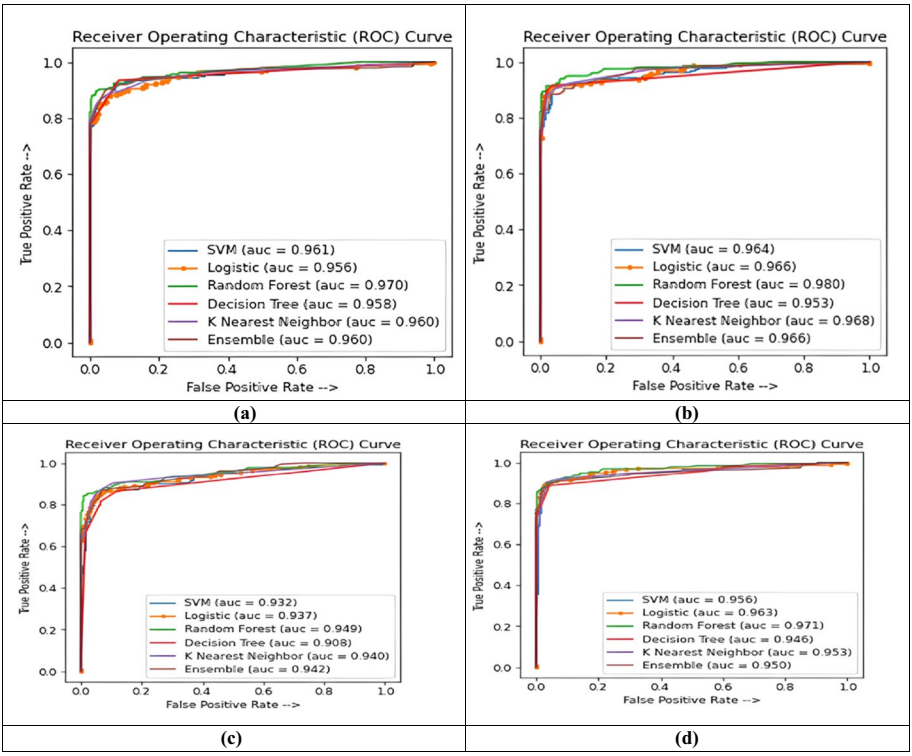

Fig. 8 A ROC curve that combines the outcomes of various classifiers that use a splitting method, (**a**) With least cost of **0.81045** (PS 5), (**b**) With least cost of **0.85425** (PS 10), (**c**) With least cost of **0.82395** (PS 15), (**d**) With least cost of **0.75206** (PS 20)

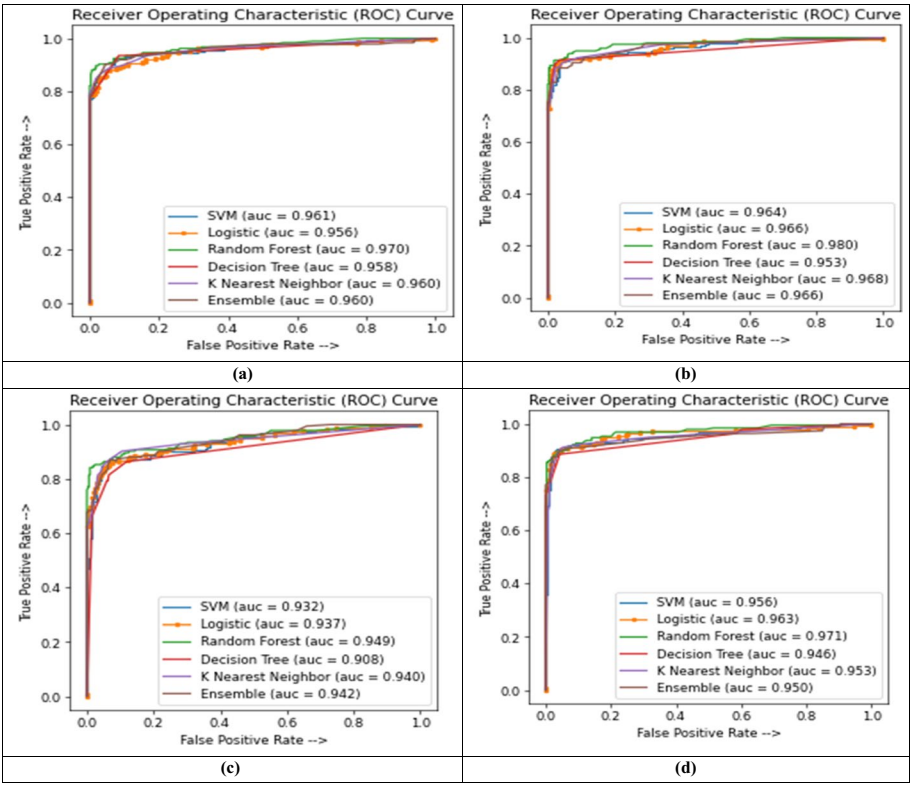

Fig. 9 ROC curves of multiple classifiers combined using a splitting approach, (**a**) With least cost of **0.81865** (PS 5), (**b**) With least cost of **0.88075** (PS 10), (**c**) With least cost of **0.76834** (PS 15), (**d**) With least cost of **0.83461** (PS 20)

Abbreviations AUC: Area Under Curve; BFO: Bacterial Foraging Optimization; CAD: Computer-Assisted Diagnosis; CDR: Cup-to-disc Ratio.; CNN: Convolutional Neural Network; DDLS: Disc Damage Likelihood Scale; DWT: Discrete Wavelet Transform; EPO: Emperor Penguin Optimization; FOS: First Order Statistical; FS: Feature Selection; GAN: Generative Adversarial Network; GLCM: Grey Level Co-occurrence Matrix; GLRM: Grey Level Run Length Matrix; HOC: Higher Order Cumulant; HOS: Higher Order Spectral; NRR: Neuro Retinal Rim; OC: Optic Cup; OD: Optic Disk; SVM: Support Vector Machine; VGG-19: Visual Geometry Group 19

Funding The authors declare that no funds, grants, or other support were received during the preparation of this manuscript.

Availability of data and materials The datasets analyzed during the current study are easily and publically available in the internet's repository.

Code availability The code is available upon request from the corresponding author for research and collaboration purposes

We also confirm that data will be available on demand

Declarations

Competing interests The authors have no relevant financial or non-financial interests to disclose. The authors declare that they have no known competing financial or personal relationships that could be viewed as influencing the work reported in this paper.

References

1. Mafarja MM, Mirjalili S (2017) Hybrid whale optimization algorithm with simulated annealing for feature selection. Neurocomputing 260:302–312. https://doi.org/10.1016/j.neucom.2017.04.053
2. Saraswat M, Arya KV (2014) Feature selection and classification of leukocytes using random forest. Med Biol Eng Comput 52(12):1041–1052. https://doi.org/10.1007/s11517-014-1200-8
3. Wei J, Zhang R, Yu Z, Hu R, Tang J, Gui C, Yuan Y (2017) A BPSO-SVM algorithm based on memory renewal and enhanced mutation mechanisms for feature selection. Appl Soft Comput 58:176–192. https://doi.org/10.1016/j.asoc.2017.04.061
4. Singh LK, Khanna MA (2022) novel multimodality based dual fusion integrated approach for efficient and early prediction of glaucoma. Biomed Sign Process Control 73:103468. https://doi.org/10.1016/j.bspc.2021.103468
5. Anoop V, Bipin PR (2020) Super-resolution based automatic diagnosis of retinal disease detection for clinical applications. Neural Process Lett 52(2):1155–1170. https://doi.org/10.1007/s11063-020-10292-x
6. Singh LK, Khanna M, Thawkar S (2022b) A novel hybrid robust architecture for automatic screening of glaucoma using fundus photos, built on feature selection and machine learning-nature driven computing. Expert Syst e13069. https://doi.org/10.1111/exsy.13069
7. Singh LK, Khanna M, Garg H, Singh R (2023). Efficient feature selection based novel clinical decision support system for glaucoma prediction from retinal fundus images. Med Eng Phys 104077. https://doi.org/10.1016/j.medengphy.2023.104077
8. Juneja M, Thakur S, Wani A, Uniyal A, Thakur N, Jindal P (2020a) DC-Gnet for detection of glaucoma in retinal fundus imaging. Mach Vis Applic 31(5):1–14. https://doi.org/10.1007/s00138-020-01085-2
9. Juneja M, Thakur N, Thakur S, Uniyal A, Wani A, Jindal P (2020b) GC-NET for classification of glaucoma in the retinal fundus image. Mach Vis Applic 31(5):1–18. https://doi.org/10.1007/s00138-020-01091-4
10. Sharma A, Dua G, Mulaveesala R (2019) Breast cancer detection using frequency modulated thermal wave imaging. Imaging Sci J 67(7):396–406. https://doi.org/10.1080/13682199.2019.1679442
11. Gupta A, Singh A (2022) An intelligent healthcare cyber physical framework for encephalitis diagnosis based on information fusion and soft-computing techniques. New Gener Comput 40(4):1093–1123. https://doi.org/10.1007/s00354-022-00175-1
12. Karadeniz T, Tokdemir G, Maraş HH (2021) Ensemble methods for heart disease prediction. New Gener Comput 39(3–4):569–581. https://doi.org/10.1007/s00354-021-00124-4
13. Zhang L (2023) A feature selection method using conditional correlation dispersion and redundancy analysis. Neural Process Lett 1-35. https://doi.org/10.1007/s11063-023-11256-7
14. Elangovan P, Nath MK (2022) En-ConvNet: A novel approach for glaucoma detection from color fundus images using ensemble of deep convolutional neural networks. Int J Imaging Syst Technol 32(6):2034–2048. https://doi.org/10.1002/ima.22761
15. Kar MK, Neog DR, Nath MK (2022) Retinal Vessel Segmentation Using Multi-Scale Residual Convolutional Neural Network (MSR-Net) Combined with Generative Adversarial Networks. Circ Syst Sign Process 1-30. https://doi.org/10.1007/s00034-022-02190-5
16. Shyamalee T, Meedeniya D (2022) Glaucoma detection with retinal fundus images using segmentation and classification. Mach Intell Res 19(6):563–580. https://doi.org/10.1007/s11633-022-1354-z
17. Singh PB, Singh P, Dev H (2023) Optimized convolutional neural network for glaucoma detection with improved optic-cup segmentation. Adv Eng Softw 175:103328. https://doi.org/10.1016/j.advengsoft.2022.103328
18. Panahi A, Askari Moghadam R, Tarvirdizadeh B, Madani K (2022). Simplified u-net as a deep learning intelligent medical assistive tool in glaucoma detection. Evol Intell 1-12. https://doi.org/10.1007/s12065-022-00775-2

19. Gampala V, Maram B, Vigneshwari S, Cristin R (2022) Glaucoma detection using hybrid architecture based on optimal deep neuro fuzzy network. Int J Intell Syst 37(9):6305–6330. https://doi.org/10.1002/int.22845
20. Singh A, Dutta MK, ParthaSarathi M, Uher V, Burget R (2016) Image processing based automatic diagnosis of glaucoma using wavelet features of segmented optic disc from fundus image. Comput Methods Programs Biomed 124:108–120. https://doi.org/10.1016/j.cmpb.2015.10.010
21. Raghavendra U, Bhandary SV, Gudigar A, Acharya UR (2018) Novel expert system for glaucoma identification using non-parametric spatial envelope energy spectrum with fundus images. Biocybern Biomed Eng 38(1):170–180. https://doi.org/10.1016/j.bbe.2017.11.002
22. Maheshwari S, Pachori RB, Kanhangad V, Bhandary SV, Acharya UR (2017) Iterative variational mode decomposition based automated detection of glaucoma using fundus images. Comput Biol Med 88:142–149
23. Krishnan MMR, Faust O (2013) Automated glaucoma detection using hybrid feature extraction in retinal fundus images. J Mech Med Biol 13(01):1350011. https://doi.org/10.1142/S0219519413500115
24. Agrawal DK, Kirar BS, Pachori RB (2019) Automated glaucoma detection using quasi-bivariate variational mode decomposition from fundus images. IET Image Process 13(13):2401–2408. https://doi.org/10.1049/iet-ipr.2019.0036
25. Kausu TR, Gopi VP, Wahid KA, Doma W, Niwas SI (2018) Combination of clinical and multiresolution features for glaucoma detection and its classification using fundus images. Biocybern Biomed Eng 38(2):329–341. https://doi.org/10.1016/j.bbe.2018.02.003
26. Shanmugam P, Raja J, Pitchai R (2021) An automatic recognition of glaucoma in fundus images using deep learning and random forest classifier. Appl Soft Comput 109:107512
27. Gour N, Khanna P (2020) Automated glaucoma detection using GIST and pyramid histogram of oriented gradients (PHOG) descriptors. Pattern Recogn Lett 137:3–11. https://doi.org/10.1016/j.patrec.2019.04.004
28. Dinç B, Kaya Y (2023) A novel hybrid optic disc detection and fovea localization method integrating region-based convnet and mathematical approach. Wireless Personal Commun 129(4):2727–2748. https://doi.org/10.1007/s11277-023-10255-0
29. Kaya Y (2020) A novel method for optic disc detection in retinal images using the cuckoo search algorithm and structural similarity index. Multimedia Tools Applic 79(31–32):23387–23400. https://doi.org/10.1007/s11042-020-09080-5
30. He C, Li K, Zhang Y, Xu G, Tang L, Zhang Y, ..., Li X (2023). Weakly-Supervised Concealed Object Segmentation with SAM-based Pseudo Labeling and Multi-scale Feature Grouping. *arXiv preprint* arXiv:2305.11003
31. He C, Li K, Zhang Y, Tang L, Zhang Y, Guo,Z, Li X (2023). Camouflaged object detection with feature decomposition and edge reconstruction. In *Proceedings of the IEEE/CVF Conference on Computer Vision and Pattern Recognition* (pp. 22046-22055)
32. He C, Li K, Xu G, Yan J, Tang L, Zhang Y, ..., Li X (2023). Hqg-net: Unpaired medical image enhancement with high-quality guidance. IEEE Trans Neural Netw Learn Syst. https://doi.org/10.1109/TNNLS.2023.3315307
33. He C, Li K, Zhang Y, Zhang Y, Guo Z, Li X, ..., Yu F (2023). Strategic preys make acute predators: Enhancing camouflaged object detectors by generating camouflaged objects. *arXiv preprint* arXiv:2308.03166.
34. Singh LK, Khanna M, Thawkar S, Singh R (2023). A novel hybridized feature selection strategy for the effective prediction of glaucoma in retinal fundus images. Multimedia Tools Applic 1-73. https://doi.org/10.1007/s11042-023-17081-3
35. Zhang L, Tang L, Xia M, Cao G (2023) The application of artificial intelligence in glaucoma diagnosis and prediction. Front Cell Dev Biol 11:1173094. https://doi.org/10.3389/fcell.2023.1173094
36. Raju M, Shanmugam KP, Shyu CR (2023) Application of Machine Learning Predictive Models for Early Detection of Glaucoma Using Real World Data. Appl Sci 13(4):2445. https://doi.org/10.3390/app13042445
37. Singh LK, Khanna M, Thawkar S, Singh R (2023). Nature-inspired computing and machine learning based classification approach for glaucoma in retinal fundus images. Multimedia Tools Applic 1-49. https://doi.org/10.1007/s11042-023-15175-6
38. Cheng J, Liu J, Xu Y, Yin F, Wong DWK, Tan NM, ...,Wong TY (2013) Superpixel classification based optic disc and optic cup segmentation for glaucoma screening. IEEE Trans Med Imaging 32(6):1019-1032. https://doi.org/10.1109/TMI.2013.2247770

39. Kolář R, Jan J (2008) Detection of glaucomatous eye via color fundus images using fractal dimensions. Radioengineering 17(3):109–114
40. Singh LK, Pooja, Garg H, Khanna M (2022) Deep learning system applicability for rapid glaucoma prediction from fundus images across various data sets. Evolv Syst 13(6):807–836
41. Raja C, Gangatharan N (2013) Glaucoma detection in fundal retinal images using trispectrum and complex wavelet-based features. Eur J Sci Res 97(1):159–171
42. Kirar BS, Agrawal DK (2018) Glaucoma diagnosis using discrete wavelet transform and histogram features from fundus image. Int J Eng Technol 7(4):2546–2551. https://doi.org/10.14419/ijet.v7i4.14809
43. Kirar BS, Agrawal DK (2019) Computer aided diagnosis of glaucoma using discrete and empirical wavelet transform from fundus images. IET Image Process 13(1):73–82. https://doi.org/10.1049/iet-ipr.2018.5297
44. Yadav D, Sarathi MP, Dutta MK (2014) Classification of glaucoma based on texture features using neural networks. In *2014 Seventh International Conference on Contemporary Computing (IC3)*, (pp. 109-112). IEEE. https://doi.org/10.1109/IC3.2014.6897157
45. Maheshwari S, Pachori RB, Acharya UR (2016) Automated diagnosis of glaucoma using empirical wavelet transform and correntropy features extracted from fundus images. IEEE J Biomed Health Inform 21(3):803–813. https://doi.org/10.1109/JBHI.2016.2544961
46. Martins J, Cardoso JS, Soares F (2020) Offline computer-aided diagnosis for Glaucoma detection using fundus images targeted at mobile devices. Comput Methods Programs Biomed 192:105341. https://doi.org/10.1016/j.cmpb.2020.105341
47. Parashar D, Agrawal DK (2020) Automated classification of glaucoma stages using flexible analytic wavelet transform from retinal fundus images. IEEE Sensors J 20(21):12885–12894. https://doi.org/10.1109/JSEN.2020.3001972
48. Acharya UR, Dua S, Du X, Chua CK (2011) Automated diagnosis of glaucoma using texture and higher order spectra features. IEEE Trans Inform Technol Biomed 15(3):449–455. https://doi.org/10.1109/TITB.2011.2119322
49. Dua S, Acharya UR, Chowriappa P, Sree SV (2011) Wavelet-based energy features for glaucomatous image classification. IEEE Trans Inform Technol Biomed 16(1):80–87. https://doi.org/10.1109/TITB.2011.2176540
50. Mookiah MRK, Acharya UR, Lim CM, Petznick A, Suri JS (2012) Data mining technique for automated diagnosis of glaucoma using higher order spectra and wavelet energy features. Knowl-Based Syst 33:73–82. https://doi.org/10.1016/j.knosys.2012.02.010
51. Noronha KP, Acharya UR, Nayak KP, Martis RJ, Bhandary SV (2014) Automated classification of glaucoma stages using higher order cumulant features. Biomed Sign Process Control 10:174–183. https://doi.org/10.1016/j.bspc.2013.11.006
52. Acharya UR, Ng EYK, Eugene LWJ, Noronha KP, Min LC, Nayak KP, Bhandary SV (2015) Decision support system for the glaucoma using Gabor transformation. Biomed Sign Process Control 15:18–26. https://doi.org/10.1016/j.bspc.2014.09.004
53. Issac A, Sarathi MP, Dutta MK (2015) An adaptive threshold based image processing technique for improved glaucoma detection and classification. Comput Methods Programs Biomed 122(2):229–244. https://doi.org/10.1016/j.cmpb.2015.08.002
54. Salam AA, Khalil T, Akram MU, Jameel A, Basit I (2016) Automated detection of glaucoma using structural and non structural features. Springerplus 5:1–21. https://doi.org/10.1186/s40064-016-3175-4
55. Haleem MS, Han L, Hemert JV, Fleming A, Pasquale LR, Silva PS, ..., Aiello LP (2016) Regional image features model for automatic classification between normal and glaucoma in fundus and scanning laser ophthalmoscopy (SLO) images. J Med Syst 40:1-19. https://doi.org/10.1007/s10916-016-0482-9
56. Claro M, Santos L, Silva W, Araújo F, Moura N, Macedo A (2016) Automatic glaucoma detection based on optic disc segmentation and texture feature extraction. Clei Electron J 19(2):5–5. https://doi.org/10.19153/cleiej.19.2.4
57. de Sousa JA, de Paiva AC, Sousa de Almeida JD, Silva AC, Junior GB, Gattass M (2017) Texture based on geostatistic for glaucoma diagnosis from fundus eye image. Multimedia Tools Applic 76:19173–19190. https://doi.org/10.1007/s11042-017-4608-y

58. Koh JE, Acharya UR, Hagiwara Y, Raghavendra U, Tan JH, Sree SV, ..., Tong L (2017) Diagnosis of retinal health in digital fundus images using continuous wavelet transform (CWT) and entropies. Comput Biol Med 84:89-97. https://doi.org/10.1016/j.compbiomed.2017.03.008
59. Septiarini A, Khairina DM, Kridalaksana AH, Hamdani H (2018) Automatic glaucoma detection method applying a statistical approach to fundus images. Healthcare Inform Res 24(1):53–60. https://doi.org/10.4258/hir.2018.24.1.53
60. Selvathi D, Prakash NB, Gomathi V, Hemalakshmi GR (2018) Fundus image classification using wavelet based features in detection of glaucoma. Biomed Pharmacol J 11(2):795–805. https://doi.org/10.13005/bpj/1434
61. Kanse SS, Yadav DM (2020) HG-SVNN: harmonic genetic-based support vector neural network classifier for the glaucoma detection. J Mech Med Biol 20(01):1950065. https://doi.org/10.1142/S0219519419500659
62. Renukalatha S, Suresh KV (2019) Classification of glaucoma using simplified-multiclass support vector machine. Biomedi Engin: Applic Basis Communic 31(05):1950039. https://doi.org/10.4015/S101623721950039X
63. Jerith GG, Kumar PN (2020) Recognition of Glaucoma by means of gray wolf optimized neural network. Multimedia Tools Applic 79(15):10341–10361. https://doi.org/10.1007/s11042-019-7224-1
64. Krishnamoorthi N, Chinnababu VK (2019) Hybrid feature vector based detection of Glaucoma. Multimedia Tools Applic 78:34247–34276. https://doi.org/10.1007/s11042-019-08249-x
65. Araújo JDL, Souza JC, Neto OPS, de Sousa JA, de Almeida JDS, de Paiva AC, ..., Gattass M (2019) Glaucoma diagnosis in fundus eye images using diversity indexes. Multimedia Tools Applic 78:12987-13004. https://doi.org/10.1007/s11042-018-6429-z
66. Thakur N, Juneja M (2020) Classification of glaucoma using hybrid features with machine learning approaches. Biomed Sign Process Control 62:102137. https://doi.org/10.1016/j.bspc.2020.102137
67. Elangovan P, Nath MK, Mishra M (2020) Statistical parameters for glaucoma detection from color fundus images. Proc Comput Sci 171:2675–2683. https://doi.org/10.1016/j.procs.2020.04.290
68. Kirar BS, Agrawal DK, Kirar S (2022) Glaucoma detection using image channels and discrete wavelet transform. IETE J Res 68(6):4421–4428. https://doi.org/10.1080/03772063.2020.1795934
69. Khan SI, Choubey SB, Choubey A, Bhatt A, Naishadhkumar PV, Basha MM (2022) Automated glaucoma detection from fundus images using wavelet-based denoising and machine learning. Concurrent Eng 30(1):103–115. https://doi.org/10.1177/1063293X211026620
70. Das S, Biswas A, Dasgupta S, Abraham A (2009) Bacterial foraging optimization algorithm: theoretical foundations, analysis, and applications. Foundations of computational intelligence, 3rd edn. Springer, Berlin, Heidelberg, pp 23–55
71. Chen YP, Li Y, Wang G, Zheng YF, Xu Q, Fan JH, Cui XT (2017) A novel bacterial foraging optimization algorithm for feature selection. Expert Syst Applic 83:1–17
72. Dhiman G, Kumar V (2018) Emperor penguin optimizer: a bio-inspired algorithm for engineering problems. Knowl-Based Syst 159:20–50
73. Keerthana D, Venugopal V, Nath MK, Mishra M (2023) Hybrid convolutional neural networks with SVM classifier for classification of skin cancer. Biomed Eng Adv 5:100069. https://doi.org/10.1016/j.bea.2022.100069
74. Singh LK, Khanna M, Thawkar S, Singh R (2022) Collaboration of features optimization techniques for the effective diagnosis of glaucoma in retinal fundus images. Adv Eng Softw 173:103283. https://doi.org/10.1016/j.advengsoft.2022.103283
75. Guo F, Mai Y, Zhao X, Duan X, Fan Z, Zou B, Xie B (2018) Yanbao: a mobile app using the measurement of clinical parameters for glaucoma screening. IEEE Access 6:77414–77428. https://doi.org/10.1109/ACCESS.2018.2882946
76. Liu S, Hong J, Lu X, Jia X, Lin Z, Zhou Y, ..., Zhang H (2019) Joint optic disc and cup segmentation using semi-supervised conditional GANs. Comput Biol Med 115:103485. https://doi.org/10.1016/j.compbiomed.2019.103485
77. Fu H, Cheng J, Xu Y, Liu J (2019) Glaucoma detection based on deep learning network in fundus image. Deep Learning and Convolutional Neural Networks for Medical Imaging and Clinical Informatics. Springer, Cham, pp 119–137. https://doi.org/10.1007/978-3-030-13969-8_6
78. Sreng S, Maneerat N, Hamamoto K, Win KY (2020) Deep learning for optic disc segmentation and glaucoma diagnosis on retinal images. Appl Sci 10(14):4916. https://doi.org/10.3390/app10144916

79. Orlando JI, Fu H, Breda JB, van Keer K, Bathula DR, Diaz-Pinto A et al (2020) REFUGE Challenge: A unified framework for evaluating automated methods for glaucoma assessment from fundus photographs[J]. Med Image Anal 59:101570. https://doi.org/10.1016/j.media.2019.101570
80. Guo F, Li W, Tang J, Zou B, Fan Z (2020) Automated glaucoma screening method based on image segmentation and feature extraction. Med Biolog Eng Comput 58(10):2567–2586. https://doi.org/10.1007/s11517-020-02237-2
81. Abad PF, Coronado-Gutierrez D, Lopez C, Burgos-Artizzu XP (2021) Glaucoma patient screening from online retinal fundus images via Artificial Intelligence. *medRxiv*
82. Elangovan P, Nath MK (2021) Glaucoma assessment from color fundus images using convolutional neural network. Int J Imaging Syst Technol 31(2):955–971. https://doi.org/10.1002/ima.22494
83. Tulsani A, Kumar P, Pathan S (2021) Automated segmentation of optic disc and optic cup for glaucoma assessment using improved UNET++ architecture. Biocybern Biom Eng. https://doi.org/10.1016/j.bbe.2021.05.011
84. Juneja M, Singh S, Agarwal N, Bali S, Gupta S, Thakur N, Jindal P (2020) Automated detection of Glaucoma using deep learning convolution network (G-net). Multimedia Tools Applic 79(21):15531–15553. https://doi.org/10.1007/s11042-019-7460-4
85. Kirar BS, Agrawal DK, Kirar S (2020) Glaucoma detection using image channels and discrete wavelet transform. IETE J Res 1-8. https://doi.org/10.1080/03772063.2020.1795934
86. Singh LK, Khanna M, Thawkar S (2022) A novel hybrid robust architecture for automatic screening of glaucoma using fundus photos, built on feature selection and machine learning-nature driven computing. Expert Syst 39(10):e13069. https://doi.org/10.1111/exsy.13069
87. Singh LK, Khanna M (2022) A novel multimodality based dual fusion integrated approach for efficient and early prediction of glaucoma. Biomed Sign Process Control 73:103468. https://doi.org/10.1016/j.bspc.2021.103468
88. Singh LK, Khanna M, Thawkar S, Singh R (2022) Collaboration of features optimization techniques for the effective diagnosis of glaucoma in retinal fundus images. Adv Eng Softw 173:103283. https://doi.org/10.1016/j.advengsoft.2022.103283

Publisher's Note Springer Nature remains neutral with regard to jurisdictional claims in published maps and institutional affiliations.

Software and Hardware Specifications: Operating System: Windows 10; Programming Language: Python 3.8.8 with Frameworks: TensorFlow 2.0; Machine Learning Libraries: Scikit-Learn, NumPy, Keras and TensorFlow; Text Editor/IDE: Jupyter Notebook (6.3.0) /Spyder (4.2.5) with Google Colab; Data Preprocessing Tools: OpenCV, etc.; CPU Model: Intel Core i7; RAM: 8 GB; Storage: 1TB. The memory required by the program(code) to execute is in KBs(for variables and other functions within the code).

Springer Nature or its licensor (e.g. a society or other partner) holds exclusive rights to this article under a publishing agreement with the author(s) or other rightsholder(s); author self-archiving of the accepted manuscript version of this article is solely governed by the terms of such publishing agreement and applicable law.

Authors and Affiliations

Law Kumar Singh[1] · Munish Khanna[2] · Rekha Singh[3]

✉ Law Kumar Singh
lawkumarcs1@gmail.com

Munish Khanna
munishkhanna.official@rocketmail.com

Rekha Singh
singh.rekha70@gmail.com

[1] Department of Computer Engineering and Applications, GLA University, Mathura 281406, India

[2] School of Computing Science and Engineering, Galgotias University, Greater Noida, Gautam Budh Nagar 203201, India

[3] Department of Physics, Uttar Pradesh Rajarshi Tandon Open University, Prayagraj, Uttar Pradesh, India